THE HAGUE UNIVERSITY OF APPLIED SCIENCES

Drinking water pellet-softening modelling

‘’Investigation to find alternatives for the use of particle size in prediction models’

Aisha Malik

Graduation Research project

Author:

Aisha Malik

Company

Waternet, Sector Drinkwater, Department Production

Team Water Quality and Process Support

Facility Weesperkarspel

Driemondweg 21

1108 AJ Amsterdam Zuidoost

Supervisors Waternet

Onno Kramer

Michel Colin

Fenna Philipse

Bachelor Chemical Engineering/Process food Technology

The Hague University of Applied Sciences

Johanna Westerdijkplein 75, 2521 EN Den Haag

Supervisor The Hague University of Applied Sciences

Caroline Mok

Acknowledgment

Over the past five months, I have had the opportunity to work with a variety of people across Waternet. Working with such capable and accomplished individuals has been a time well spent that I am very grateful for.

Waternet has given me a fascinating and ideal work environment with an awesome bunch of colleagues that proven to be very supportive. At first, I would like to convey my special gratitude to the entire Water Quality team especially Leon Kors, for giving me this opportunity despite the challenging Covid 19 circumstances. I would also like to express my sincere thanks towards Michel Colin, for his constant guidance and support that has helped me strengthen my skillset. The completion of my graduation project would not have been possible without the valuable support of Mark Joosten, and Peter Wind, who despite their busy schedules have taken the time and effort to source the required machinery and apparatus to enable the experiments. The advice provided by Fenna Philips, in the early stages of the project and her constant feedback has been pivotal in the completion of my project.

Special thanks to my university supervisor Caroline Mok Kai Rine, for her constant guidance and her value able feedback. Lectures provided by her on the related topic has helped me to understand graduation assignment. I would like to thank Roy Duijnmaijer, my fellow graduate intern at Waternet, for always lending a helping hand and to Eric Baars, for taking the time to provide feedback and support on the theoretical and as well as practical aspect of the project.

I had always wanted to do my graduation internship on a topic that is interesting yet challenging with a special focus on drinking water. And would finally like to convey my heartfelt thanks to Onno Kramer for providing me the opportunity to do so. Onno, you have been a source of great inspiration to me and I cannot thank you enough. I have been bedazzled by your knowledge and drive. Your gentle guidance and mentoring have helped me grow as an engineer as well as a person.

Last but not the least, I would like to thank my mother, Sajida Azeem, my brother Ibrahim Malik, and my husband and soulmate, Umar Waleed Malik, for being my anchors and always been there for me. You are precious.

Abstract

Drinking water utilities are responsible for providing safe drinking water. As water directly impacts public health, water utilities follow stringent water treatment standards and processes. However to keep pace with the dynamic environment and tackle challenges such as water stress, water pollution, climate change, and sustainability, water utilities are required to adapt their processes. In order to adapt, careful research is done beforehand on its consequences. Amongst others, prediction models are used to foresee these consequences.

Waternet is a water utility in Amsterdam (The Netherlands) that uses natural grains in their multiphase flow processes such as pellet-softening, slow sand filtration and rapid sand filtration. While these natural grains are non-spherical in shape, most prediction models assume the input of perfect spheres and correct by applying a particle shape correction factor. This research aims to focus on how to account for non-spherical particles.

Literature investigation is performed on how to account for non-spherical particles in a voidage prediction model which showed that no general agreement or consensus is illustrated in the literature accounting for particle shapes and size in a voidage prediction model. Operational field of water treatment lies in the vicinity of incipient fluidisation and laminar/transitional regime is preferred therefore, a conventional model such as Carman-Kozeny is used, and the new empirical data-driven model to find out the estimated spherical diameter for non-spherical particles by using the experimental data collected from expansion experiments.

All lab experiments for spherical glass beads (0.8-3.5 mm) and non-spherical glass rods (3x9 mm) were conducted at a wide range of 5-35 degrees Celsius, simulating the seasonal water temperature range at Waternet and beyond. The results of the experimental work have shown that particles used by the treatment plants are dependent on flow and it has an effect on the expansion behaviour which can effect crystallisation process in pellet softening process. Nevertheless, spherical particles are independent of flow. Furthermore, it has been shown that the new empirical data-driven model which is applicable for spherical particles does not work well for non-spherical particles. The present research has also focused on the orientation of the non-spherical particles which change with fluid flow rate. The dimensionless number approach has been applied to experimental data of non-spherical glass beads using Carman-Kozeny drag relations. It has been found that the Carman-Kozeny constant is not constant in a fixed and fluidised bed state. Mostly, the shape factor is applied only in the fixed bed state but in the fluidised state it is simply omitted. Nevertheless, with the help of experimental data, the dynamic shape factor has now been determined in the fixed as well as in the fluidised state.

Table of contents

1 Introduction

This chapter explains water hardness and includes a brief description of the company, Waternet. Further, there is some overview of drinking water treatment by Waternet at its different facilities. Later on, the link between water treatment and multiphase flow is discussed which is further elaborated by liquid-solid fluidisation using pellet-softening as an example. Furthermore, the sustainability goal is discussed, and then desired situation for the present research is focused on by specifying and establishing the main research question with a few sub-questions.

1.1 Water hardness

Rainwater and surface water are soft compared to underground water where it percolates through the rocks and picks up natural hardness minerals like magnesium and calcium. The natural organic breakdown results in (CO_2) formation and the substantial dissolution of limestone and forms the Ca^{2+} and HCO_3^- (P.J.de Moel, 2006). On the other hand, the underground water stays for a long residence time in chemical equilibrium, i.e. calcium carbonate equilibrium and when it is pumped to the surface and it comes in contact with air, carbon dioxide (CO_2) disappears and calcium carbonate ($CaCO_3$) equilibrium is disturbed. Moreover, when water is heated at household equilibrium changes again, as the bicarbonate (HCO_3^-) will convert to carbonate and precipitates out with calcium (Ca^{2+}) in the form of calcium carbonate ($CaCO_3$), which lead to inconveniences like scaling of calcium carbonate on the home appliances, extra use of soap and detergents, deposits on water boilers. To manage this undesired situation which is known as water hardness, water companies give their best to partially removed calcium ions from the water.

1.2 Waternet

Waternet is the only water company that covers the whole water cycle in the Netherland (Who We Are) Water cycle activities include drinking water treatment and distribution, wastewater collection and treatment, and water system management and control (van der Hoek, 2012). Societal call and drive towards the need to be sustainable has also made water utilities carbon neutral and minimise chemical usage as much as possible. Waternet has some value cores so without making any compromise on that values an aim has been set forth to be sustainable. Goals include process optimisation concerning water quality guidelines (River Basin Management - Water - Environment - European Commission) valorisation to raw materials re-use and efficient use of chemicals according to the standards in the Dutch National Drinking Water Standards (Waterleidingbesluit), saving energy, shifting to renewable energy, and compensation measures for CO_2 emissions (Beeftink et al., 2021). Among the activities, the process optimisation step is crucial for drinking water treatment as a bulk amount of chemicals are exploited in this process.

1.3 Overview of the drinking water treatment

For the production of reliable, safe, and clean water. Waternet has several treatment plants that comprise unit operations. The whole treatment consists of two steps starting from pre-treatment at Loenderveen (LVN) and main drinking water treatment at Weesperkarspel (WPK). Water from the surface of the Rhine canal and Bethune polder is collected and pre-treated at

Loenderveen before it goes to further treatment at Weesperkarspel. A series of pre-treatment includes coagulation, sedimentation, self-purification in a lake water reservoir, and rapid sand filtration. Then water is collected at Weesperkarspel through 14 kilometres pipeline without chlorination.

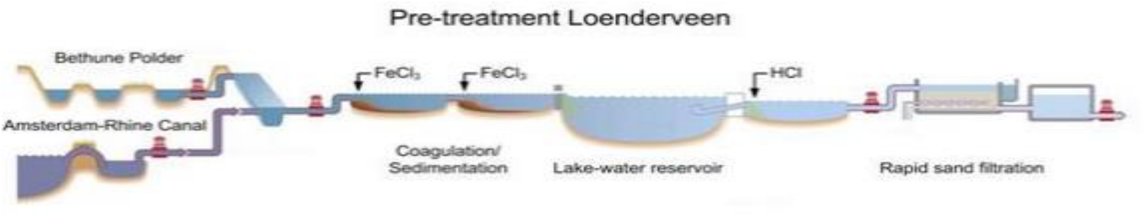

Figure 1: Pre Treatment Loenderveen (Van Schagen, 2009).

At Weesperkarspel further treatment takes place that includes disinfection and oxidation of the organic material by ozone. This is further followed by pellet-softening therefore, eight pellet reactors are in place at WPK for softening water after that, the water is transported to the biological activated carbon filtration to remove pesticides and micropollutants either by adsorption or removal by biological activity. The last step involves slow sand filtration to remove any remaining organic or inorganic particles from the treated water.

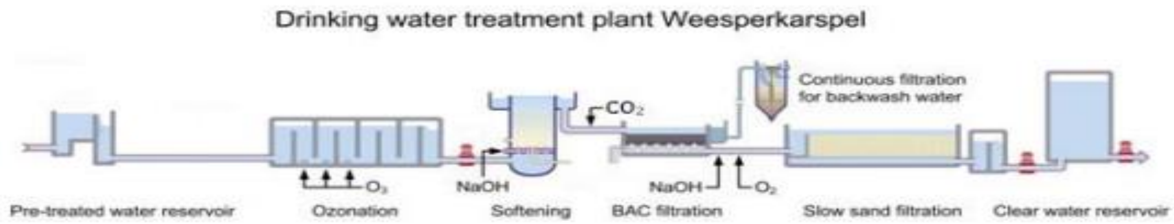

Figure 2: Drinking water treatment WPK (Van Schagen, 2009).

1.4 The Link between fluidisation and water treatment

Fluidisation is a process that is similar to liquefaction, during fluidisation the granular particles exhibit a dynamic fluid-like state from a static state (Albright, 2008). Over time many developments took place and their benefits have revolutionised the industrial field. Multiphase fluidisation is a technique where flows are composed of solid, gas and/or liquid (Gibilaro, 2001).

At Waternet treatment facility unit operations, multiphase flows are frequently encountered. Waternet uses natural or processed grains that are non-spherical particles in multiphase flow systems examples are pellet-softening (Rietveld et al., 2006a), (Van Schagen, 2009) backwashing procedures (Soyer & Akgiray, 2009), and granular activated carbon. Pellet-softening is one of the examples among many other Waternet multiphase flow processes that focuses on liquid-solid fluidisation.

1.5 Liquid-solid fluidisation

Due to its limited application compared to gas-solid fluidisation, (Di Felice, 1995), liquid-solid fluidisation is less researched and understudied in the literature compared to the most popular gas-solid fluidisation. Presently liquid-solid fluidisation is gaining more attention and becoming a more discussed and popular topic in future research as its applications are steadily increasing. It could be used for the classification of particles in terms of their sizes and densities, to fluidise catalysts to crack heavy hydrocarbons in the petroleum industry, and also as bioreactors for aerobic and anaerobic wastewater treatment (Epstein, 2002). One of the many before mentioned examples of liquid-solid fluidisation is also the seeded-crystallisation of the fluidised bed in the pellet-softening reactors (P.J.de Moel, 2006).

1.6 Pellet-softening

In the Netherlands, almost 400 million m^3 is softened annually by fluidised bed pellet reactors (Graveland et al., 1983a). Pellet-Softening which is an enticing process for water softening was developed and introduced in the Netherlands around the 1970s (Graveland et al., 1983b). At Waternet pellet-softening is always executed in reactors that are cylindrical known as pellet reactors, about eight reactors are located at WPK having a diameter of 2.6 m and a height of 5.5 m, two-third of their volume is filled with seeding material (previous garnet sand and now crushed calcite/lime pellets are used). Water is introduced from the bottom at different high velocities varies between superficial rate 60 and 90 m/h (van Schagen et al., 2008), this causes present seeding material in the reactor to fluidised. The maximum fluid bed height and capacity of each pellet reactor are 4.5 m and 4800 m^3/h. Simultaneously, an amount of 0.8-1.4 mmol/L of NaOH 25% w/w is added to achieve a pH around 9.8 at the bottom of each pellet reactors via a separate opening, dosing point (nozzles) and incoming water create turbulence at the bottom of the reactor which results in rapid mixing. Caustic soda along with water makes its way towards the upper part and causes axial mixing too. Ultimately, the solubility of the product $CaCO_3$ exceeded and it causes crystallisation on the surface of seeding materials which then grow in size and settle at the bottom and could be drawn out of the reactor (Sobhan, 2019), (Rietveld et al., 2006a). Hence, stratification of seeding grains takes place due to the instantaneous crystallisation (Maeng et al., 2016). As the calcium is removed from the water in this process, the reactor effluent has a lower pH varying between 8.5-9.2. Later it could be adjusted by adding CO_2 to the desired pH.

$$\mathrm{NaOH} + \mathrm{CO_2} \rightarrow \mathrm{HCO_3^-} + \mathrm{Na^+} \tag{1}$$

$$\mathrm{NaOH} + \mathrm{HCO_3^-} + \mathrm{Ca^{2+}} \rightarrow \mathrm{CaCO_3} + \mathrm{Na^+} + \mathrm{H_2O} \tag{2}$$

If the conditions at bottom of the reactor are not well controlled then besides the growth of crystal on the pellet, nucleation of the seeding material might occur in solution. Using the pellet-softening process the total hardness is reduced to approximately 1.4 mmol/L during the softening process (Rietveld et al., 2006b).

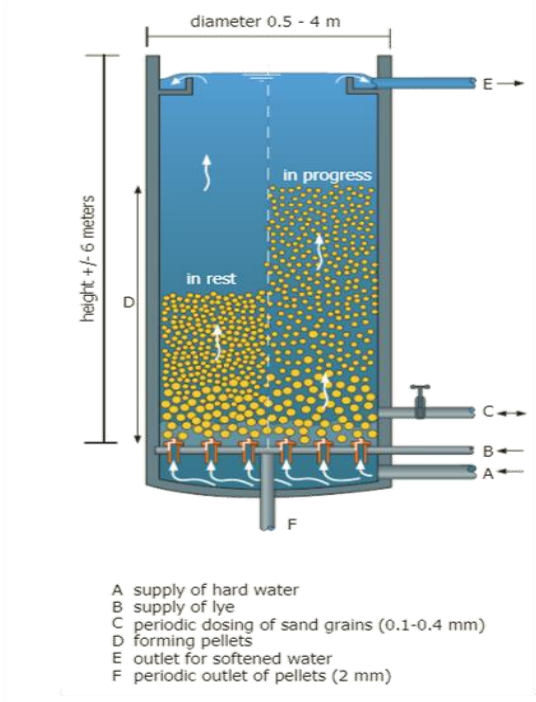

Figure 3: Pellet-softening reactor (Graveland et al., 1983b).

1.7 Sustainability goals

Since the late 1980s Waternet uses garnet sands for water softening (Graveland et al., 1983b) but to meet the sustainability goals and to decrease carbon footprints, and to become more circular instead of a linear approach, the garnet sand process could be replaced by crushed calcite/lime pellets and re-used calcites (Palmen et al 2012), the garnet sand was shipped from Australia to the Netherlands and by-product i.e. (lime pellets) has sand as centered which hindered its application to reuse as seeding material and its application in high-potential market segments such as glass and paper. The essence of eliminating most of the carbon footprints of transport and waste by-products supports $C0_2$ neutral goal (Schetters et al., 2015). From 2014 to 2016 Waternet has switched from garnet sand to locally produced calcite seeding material which is produced from (100% lime pellets) washed, crushed, and sieved. Meanwhile, usage of the by-product as raw material also reduced cost and provides aesthetic, socioeconomic, and environmental benefits in the area of pellet-softening. By now almost all the water facilities are switched to crushed calcite in the Netherland. Moreover, the use of caustic soda during pellet-softening should also be minimized (Beeftink et al., 2021) hence the amount of caustic soda needed for the removal of calcium depends on the performance of the crystallisation process inside the softening reactor. Simultaneously, the crystallisation process depends on the hydraulic conditions or, the behaviour of the fluidised bed inside the softening reactor (O.J.I. Kramer, de Moel, Padding, et al., 2020). Hence optimising the hydraulic condition of the softening reactors, supports the sustainability goal that Waternet has established for itself.

1.8 Present situation

Waternet uses natural grains in multiphase flow systems. Natural grains are assumed more spherical than self-processed grains. There was a driver to replace the non-sustainable seeding material with the more sustainable raw material. Therefore, several research projects

(Schetters et al., 2015) were conducted and there is a lot of experience within the field i.e, full-scale plant and pilot plant research was executed on applied and academic grounds, from that within few years there was a transition in a very full-scale installation. Experimentally it's been proved too, that there's not any difference using calcite grains rather than garnet sand in terms of water quality (Schetters et al., 2015). The difference between garnet and crushed calcite isn't only particle density, but garnet sand is mined and crushed calcite is processed, (ground) that includes a significant impact on particle shape.

Figure 4- Crushed calcite

The density of garnet sand is over the calcite grains and it varies too along with the height of the column as crystallisation proceeds but using calcite grains, density remains constant. Garnet sand that was used previously has a diameter of 0.25 mm offering a large specific surface area whereas, calcite grains range in size 0.5 mm-1.0 mm. Due to the turbidity, during the previous experiments, it absolutely was difficult to observed for specific surface area. Thus, to acquire the process state of the fluidised bed, the foremost important and crucial process variable, i.e. the effective specific surface area (SSA) for the aim of crystallisation, must be known. Therefore, the effective voidage must be determined. Consequently, specific surface area is also depend on particle diameter that could be seen in Equation 3. Specific surface area determination depends on the shape of particles (d_p) which is considered spherical at the moment to use in model, but in the case of crushed calcite grains, particles are extremely non-spherical. The size and shape of particles inside the softening reactor can only be determined before they are added, and after they're removed. How large, and where within the reactor the particles are during the softening process is unknown. Because of that, the surface area provided by the particle bed is unknown, which makes it impossible to accurately determine caustic soda needed for the removal of calcium ions.

$$A_s = 6\frac{1-\varepsilon}{d_p} \tag{3}$$

Where:

A_s	specific surface area	[m²/m³]
ε	bed voidage or fluid void fraction	[m³/m³]
d_p	particle diameter	[m]

1.9 Knowledge gap

Voidage depends on the fluid properties such as kinematic viscosity, superficial fluid velocity, and particle properties like particle density, and particle diameter (Yang, 2003a). In the operational field of the drinking water utilities, the natural grains are used mostly. A sieve analysis method is mostly used to measure the particle diameter. However, the use of particle diameter does not make more sense for non-spherical grains. The sieve method does not say about the particle shape. However, particle shape has influenced the hydraulics of liquid-solid fluidisation. Hence, it is desired to replace particle diameter with any morphological property in a voidage prediction model.

A knowledge gap is present that is not clear and there is not any general agreement in the literature (Onno J. I. Kramer et al., 2021) on how to include sizes and shape of irregularly non-spherical particles in expansion prediction models applied in the drinking water processes. Since the crushed calcite pellets are highly non-spherical, usually perfectly round spheres are unsuitable. It is of extreme importance to have an effective model which should be reliable enough to predict to risk of ineffective treatment processes. As any kind of ineffectiveness could be responsible to effect directly to the quality of drinking water. Therefore preliminary research is required to validate that the conventional and the new empirical model using particle diameter is not applicable for non-spherical particles.

1.10 Main research question

The desired situation could be summarised with a research question stating:

How to account for non-spherical particles in the voidage prediction model?

1.11 Sub research questions:

- Can we include the defined dimension of particles in a voidage prediction model such as objects which has defined shapes and can be described mathematically?
- Are the conventional model valid for non-spherical particles?
- Is it possible to find an alternative way to replace the particle size with another quantity, such as dimensionless numbers? Or applying shape factor?
- Overall, the goal is to improve the model prediction accuracy of voidage.

2 The theoretical basis

Removal of hardness from water is theoretically divided into chemical and physical parts. In this report, the chemical part is not a focus only the physical part would be discussed as it deals with the hydraulics of the fluidisation and the theoretical approach could be seen that are used for voidage prediction.

2.1 Hydraulics of the fluidisation

Voidage is a function of fluid properties and particle properties. In this section, basic hydraulics of fluidisation will be discussed like superficial velocity, temperature, pressure drop, density, and size of particles, etc.

2.1.1 Superficial fluid velocity

Superficial velocity is the main parameter of fluidisation hydraulics and it is defined as hypothetical fluid velocity that passes through the porous media, calculated as it is only one type of fluid flowing in a given or present cross-sectional area. With the increase of superficial velocity, the bed of grains expands and several distinct stages could be observed with naked eyes and also by looking at scale which shows the increase in bed height (Introduction to Fluidisation)

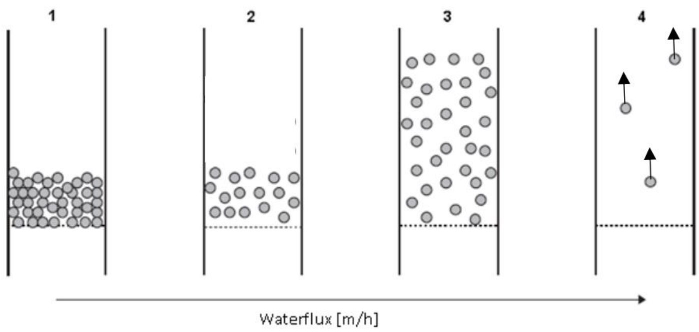

Figure 5: Expansion behaviour (O.J.I. Kramer, Boek, & Gridley, 2020)

The first stage when superficial velocity is not so effective to lift the bed upward is known as a fixed bed. At this stage granules are close to each other, stacked at the bottom, and are densely packed depends on the shape of grains. At the second stage with some increase in superficial velocity a point approaches where grains are at minimum fluidisation that could be either homogenous or heterogeneous. At this stage movement of the fluid through the empty spaces between grains which also known as voids become powerful that the grains start experiencing force which results to impart them. This transition between fixed and fluidisation state is minimal and it is followed by the third stage where further increase in fluid flow causes the granules to move away from each other. Hence, voids increase and bed expanded therefore, this phase is named expansion. The last stage is called flushing that occurs when the flow is further increased. The fluidisation process can control by varying superficial velocity and it is expressed mathematically as:

$$v_s = \frac{Q_w}{\frac{\pi}{4}D^2} \tag{4}$$

Where:

v_s	superficial velocity of water	[m/s]
D	column diameter	[m]
Q_w	water flow	[m³/s]

Open spaces between the grains are sometimes also called porosity/voidage (ε). It is a very crucial variable in fluidisation. Primarily if the mass of the granules is known and bed height then voidage can also be estimated as:

$$\varepsilon = 1 - \frac{m}{\frac{\pi}{4}D^2 L \rho_p} \tag{5}$$

Where:

ε	bed voidage or fluid void fraction	[-]
m	particle mass	[kg]
L	bed height	[m]
ρ_p	specific particle density	[kg/m³]

2.1.2 Fluid temperature

Temperature is also an important parameter for fluidisation as the dynamic viscosity depends on the fluid temperature and in the present case fluid is water. Expansion of the bed is also determined by the density of the fluid as the density of the water decreases with an increase in temperature meanwhile, dynamic viscosity also decreases. Dynamic viscosity can be calculated using the Vogel-Fulcher-Tammann Equation (Civan, 2007).

$$\eta = \frac{1}{1000}(0.83 + 0.0085\,T)^{-3} \tag{6}$$

Where:

η	dynamic viscosity of the fluid	[kg/m/s]
T	water temperature	[°C]

And:

$$\nu_T = \frac{\eta}{\rho_f} \tag{7}$$

Where:

ν_T	kinematic viscosity of the fluid	[m²/s]

2.1.3 Partial pressure difference

At fixed bed state when particles are overlapping each other until the fluidisation occurs an increase in partial pressure can be seen with increasing flow. At the minimum fluidisation point when expansion occurs pressure will remain constant. This is indicated by C in figure 8 whereas, from A t B continuous rise in pressure difference with the flow is observed. However, minimum fluidisation velocity differs for different particle beds as it depends on particle properties, size of the reactor, and viscosity of water (Gibilaro, 2001).

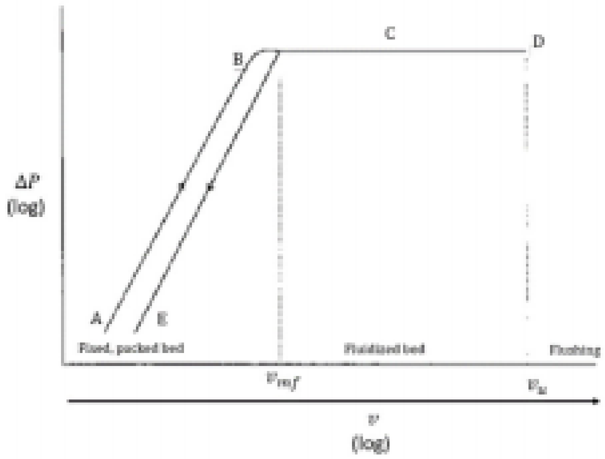

Figure 6:Differential Pressure across the bed (Gibilaro, 2001).

The pressure difference over the height of the fluidised column is used to determine porosity between the two points and that relation is given by:

$$\frac{\Delta P}{\Delta L} = \left(\rho_p - \rho_f\right)(1 - \varepsilon)\, g \qquad (8)$$

Where:

g	local gravitational field of earth equivalent to the free-fall acceleration	[m/s^2]
ΔP	differential pressure	[kPa]

the porosity can be directly calculated if ΔP, ρ_p, and ΔL are known since g, ρ_p and ρ_f are constants. Hence, the differential pressure is then the only parameter that needs to be measured for porosity.

2.1.4 Particle properties

Particle properties such as particle diameter and density are pivotal parameters in the fluidisation process as it helps in the classification of the grains in the fluidised bed. The fluidised bed is non-stationary due to the classification of the granules. Due to classification the fluidised bed is divided, as larger particles settle at the bottom whereas, smaller ones stay at the top due to their smaller diameter and density. It has illustrated by (O.J.I. Kramer, de Moel, Raaghav, et al., 2020) that the terminal settling velocity of an individual particle is a function of the diameter and particle density. It could also be observed that voidage is a function of particle property, i.e. particle density, and diameter (O. J. I. Kramer, de Moel, Padding, et al., 2020a).

2.2 Voidage prediction models

In the voidage prediction model, fluid properties and particle properties are interrelated. Such as in other multiphase, the voidage prediction model in the fluidised reactor is also given in liquid-solid fluidisation (Dharmarajah, 1982), (Yang, 2003b). In the literature, voidage prediction models are classified as porous-based media models and terminal settling models. A widely used classical approach like the (Carman-Kozeny, 1937) model is derived from the drag model where viscous and inertial forces are balanced using the modified particle Reynolds number. Voidage can also be predicted using the most widely used (Richardson-Zaki, 1954) approach that is based on terminal settling velocity.

Richardson-Zaki's approach to determining voidage is based on superficial velocity, terminal settling velocity, and together with an empirical index straightforwardly. Another prediction model (Van Schagen, 2009) to determine terminal settling velocity of calcite grains is also based on the Richardson-Zaki approach, and to predict voidage at minimum fluidisation conditions, either the minimum fluidisation velocity should be known or the Richardson-Zaki index must be very accurate, therefore an improvement for Richardson-Zaki model was made by (O.J.I. Kramer, de Moel, Padding, et al., 2020) and the model was extended on the base of proven hydraulics. On the other hand, the (Ergun, 1952) approach, to predict voidage is based on balancing between pressure gradient over the fluidised bed height due to the mass of the grains and the effect of the drag force that is exerted by the water on the particles. Additionally, quite a comprehensive data-driven model approach for voidage prediction is presented by (O. J. I. Kramer, de Moel, Padding, et al., 2020b) where a numerical method was applied to determine voidage that could be seen in 3.1.

In water treatment processes the particles that are used are relatively non-spherical and it is common to practice applying shape factors in a fixed bed state but it is omitted in a fluidised state in all conventional models (O. J. I. Kramer et al., 2020) Although, the same particles are involved in a fixed and fluidised state. For the sake of convenience, it is also commonly practiced within hydraulic modelling that the particles are often assumed as a sphere. Therefore, there is not any consensus or any agreement on how to account for the naturally irregular shape particles and to include them in the voidage prediction model for liquid-solid fluidisation. The shape descriptors approach can be used which are mathematical functions and pre-calculations are needed to determine various dimensional variables of the particle for example length, projection perimeter, volume, surface area, and diameter, etc. Sphericity is an example of such a shape descriptor. It could be seen in the literature (Wadell, 1933) describes that particle shape is commonly characterized by sphericity and it is defined as the ratio of a surface area of an equal volume sphere to the actual surface area of the particle. However, it is difficult to define shape and account for sphericity. Whereas, If the particle has a known geometric shape then it is easy to calculate sphericity mathematically.

ψ = projected area of the volume equivalent sphere/actual surface area of the particle

Sphericity is equal to 1 for spheres but it becomes less for non-spherical particles (Bagheri & Bonadonna, 2016). Furthermore experimentally it has been seen that particle orientation has also a significant impact on bed voidage due to realignment and rearrangement of the particles and the shape factor is not constant in the fluidised state it varies from 0.6 to 1.0 (Onno J. I. Kramer et al., 2021). There is an open criticism to applying shape factors in the literature, (Yang, 2003c) has added that it is difficult to classify shape factors for specific granules as different particle shapes will have the same shape factors. Another approach to account for non-spherical particles in a voidage prediction model is (Dharmarajah, 1982) where three different shape factor approaches were applied to account for non-sphericity. Whilst an effort was made by (Wen & Yu, 1966) to measure the minimum fluidisation velocity, for particles of different ranges and sizes based on experimental data. They combined it with the Ergun Equation and obtained a relation. (Akgiray & Soyer, 2006) also proposed a voidage prediction model on an improved drag with an extended evaluation of expansion Equations for a fluidised liquid-solid system. (O. J. I. Kramer et al., 2020) has demonstrated that the effective voidage for non-spherical can also be predicted by using dimensionless Froude and Reynold number on an implicit drag relation.

3 Modelling and Method

The prediction for the hydraulic fluidisation model focuses on non-spherical particles to determine accurate voidage. It is based on a empirical data-driven model determined by the experiments conducted in the pilot plant (WPK) using an expansion column.

3.1 Data-driven model

A straightforward way is to determine voidage for a particle is to use a set of the polynomial as a function of velocity, kinematic viscosity respectively, whereas particle density is considered as constant. For monodispersed glass beads (spherical shape) a model is used where porosity is a function of v_s, υ_T, ρ_p, ρ_f, and d_p (O. J. I. Kramer, de Moel, Padding, et al., 2020b). The benefits of using this modelling approach lies in the simplicity of having a single and straightforward model in which fitting parameters are obtained using non-linear regression software. Equation (9) is a straight derivation of a new empirical data-driven model and has been used for monodispersed glass beads, and Equation (*14*) is used for voidage prediction of glass rods.

$$\varepsilon = c_0 {v_s}^{c_1} {\upsilon_T}^{c_2} {d_p}^{c_3} \left(\frac{\rho_p}{\rho_f} - 1\right)^{c_4} \tag{9}$$

3.2 Preliminary exploration of adjusted data-driven model for rods

For the preliminary exploration, particle diameter for non-spherical particles could be replaced by parameters of known geometric shape. In the present research work, rod shape is selected due to availability for experimental purposes.

d_p is replaced by defined dimensions of rod Volume/Area:

$$\varepsilon = c_0 {v_s}^{c_1} {\upsilon_T}^{c_2} \left(\frac{\rho_p}{\rho_f} - 1\right)^{c_4} \left(\frac{V}{A}\right)^{c_3} \tag{10}$$

These are known factors experimentally.

For rod-like structure $\frac{V}{A}$ is further simplified where W is the width of the rod and L is the length:

$$\frac{V}{A} = \frac{\frac{\pi}{4} W^2 L}{2\frac{\pi}{4} W^2 + \pi W L} \tag{11}$$

$$\frac{V}{A} = \frac{\frac{1}{4}W^2L}{\frac{1}{2}W^2 + \pi WL} \tag{12}$$

Multiplying Equation 12 with 4, $\frac{V}{A}$ is further simplified

$$\frac{V}{A} = \frac{WL}{2W + 4L} \tag{13}$$

by putting simplified $\frac{V}{A}$ in Equation 10:

$$\varepsilon = c_0 {v_s}^{c_1} {v_T}^{c_2} \left(\frac{\rho_p}{\rho_f} - 1\right)^{c_4} \left(\frac{WL}{2W + 4L}\right)^{c_3} \tag{14}$$

Whereas v_s is the superficial fluid velocity v_T is the kinematic viscosity, ρ_p the particle density ρ_f is the fluid density and, c_0, c_1, c_2, c_3, and c_4 are the fitting parameters. It is very important to account for particle orientation too. As the present work is the first attempt towards physical hydraulic modeling, therefore, orientation will be experimentally observed but it is not part of the model due to its complexity. Simultaneously, based on the scientific work by (O. J. I. Kramer et al., 2021). It was found that there is a general (but approximated) relationship between the voidage and the particle size, i.e. c_3 = -0.30. This was based on more than 500 expansion experiments (e.g. glass pearls, steel beads shots, nylon balls but also less spherical particles like calcite pellets, etc.)

Table 1: Fitting parameters for glass beads.

Model parameter	Value
c_0	1.77
c_1	0.34
c_2	0.12
c_3	-0.30
c_4	-0.25

3.3 Method

To calibrate and validate a conventional and new empirical data-driven model for spherical and non-spherical particles, liquid-solid expansion experiments are needed. These experiments are used to obtain reliable datasets containing superficial velocity, kinematic viscosity, particle density, and diameter, etc. Therefore, an advanced pilot plant scale expansion column is used. Before conducting the experiments flow meter, the differential pressure sensor is calibrated and validated. It has to be noted that no NaOH is dosed in the expansion column.

3.4 Experimental set-up

To determine the hydraulic behaviour of the grains (spherical and non-spherical) several experiments were performed using a 4 m long expansion column in the pilot plant at Weesperkarspel, a column with a diameter of 0.057 m. The whole experimental setup is comprised of 3 pumps, each pump has a different capacity to withstand. Pump 2 is used to work with flow less than 300 L/h whereas higher flow could be attained using pump 1. Pump 3 is just a circulation pump for hot/cold water. The Flowmeter is used to measure flow rate and the control valve is used to adjust desired flow. The column is also equipped with a scale where bed height could be read easily and differential pressure sensors are present one at bottom of the column and the other at the top. Heater and cooler are used to adjust the temperature of the water. Monodispersed glass beads (spherical) are fluidised expansion behaviour is composed with graphs the same process is also followed for glass rod expansion. Possible deviation due to fluctuation of the equipment and human error could be encountered while experimenting. A complete process flow diagram of the system could be seen in supplementary material in the experimental part.

Monodispersed glass beads ranging in size 2.5 mm and 3.5 mm are fluidised at 5-6 different temperatures to see the effect of expansion at different temperatures because water suppliers that use surface water the temperature also has consequences for the process control strategies (O. J. I. Kramer, de Moel, Padding, et al., 2020b). Whereas, for glass rods due to unavailability only aspect ratio of 3 is selected and 1.5 m long glass rod is cut using a saw machine. It has been seen that the edges of the rods were not smooth but still were used for experimental purposes.

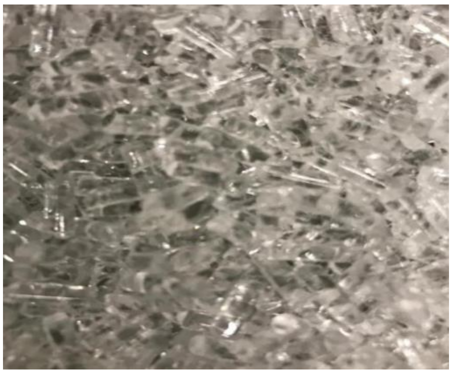

Figure 7: Glass rod aspect ratio 3.

Firstly, the particle diameter of the monodispersed glass beads was determined using sieve analysis and the micrometer. Relative information can be found within the supplementary material.

In the case of rods, the length and width are measured only using the micrometer.

After that grains were measured taking under consideration porosity 40% for spherical and 38% for non-spherical (Moghaddam et al., 2019) information related to the mass calculation and density measured using the pycnometer method can also be seen in the supplementary material.

The rods are cut in the pilot-plant lab, due to time limitations and complexity 0.7 kg of rods were collected.

At first, monodispersed glass beads (spherical) are allowed to enter the column from the top using a funnel to avoid any loss of the grains whereas, water enters from the bottom of the column.

Revised values of mass and density are filled in the Excel template (see attachment template -supplementary material). The circulation pump was turned on and desired temperature was adjusted. When all the particles reached the bottom of a column, the flow was set on a different range starting from fixed bed [0] to fluidisation [1].

Flushing of any grains was avoided.

Partial pressure, bed height, and flow were measured until they remain stable and noted in the Excel template for each measurement.

The flow was increased slowly to get enough measurements and after that, it is slowly decreased to zero using a control valve and the pump is turned out. Filter was checked at the end for possibly flushed particles.

After experimenting with spherical glass beads the same method is followed for glass rods and experimental values are noted in the Excel template for voidage calculation. An example of template for the experimental data can be found within the supplementary material.

Figure 8: Expansion column setup at Weesperkarspel, Amsterdam.

4 Results and Discussions

In this part of the report, the results are graphically explored and are discussed. In Section 4.1 expansion behaviour of monodispersed glass beads 2.5 mm is discussed. Then, in Section 4.2 particle size for monodispersed glass beads has been determined using conventional model Carman-Kozeny and new empirical data-driven model. However, in Section 4.3 expansion behaviour of glass rods have been graphically explored and discussed with spherical particle diameter determination and validity of voidage prediction model. Afterward, in Section 4.4 the drag is determined based on modified particle Reynolds number. Finally, in the Section 4.5 dynamic shape factor approach is discussed.

The data is obtained from set of expansion experiments conducted with two different shapes of particles in the expansion column separately, at the Weesperkarspel drinking water pilot plant located in Amsterdam, the Netherlands. At first monodispersed spherical glass beads Figure 9 and Figure 10 illustrates expansion behaviour for monodispersed glass beads. Secondly, Figure 14, and Figure 14, show an expansion of glass rods. These expansion curves are composed by measuring the sequence of differential pressure, the flow rates, and temperatures, etc.

4.1 Graphical exploration monodispersed glass beads

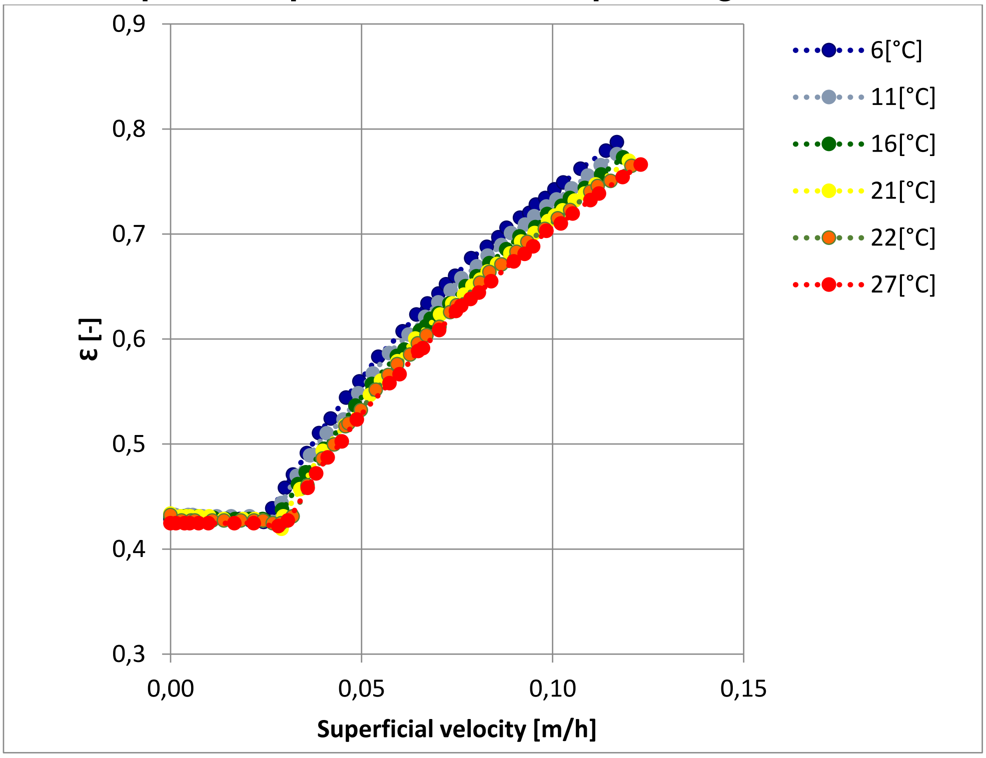

Figure 9: Expansion curve monodispersed glass beads 2.5 mm.

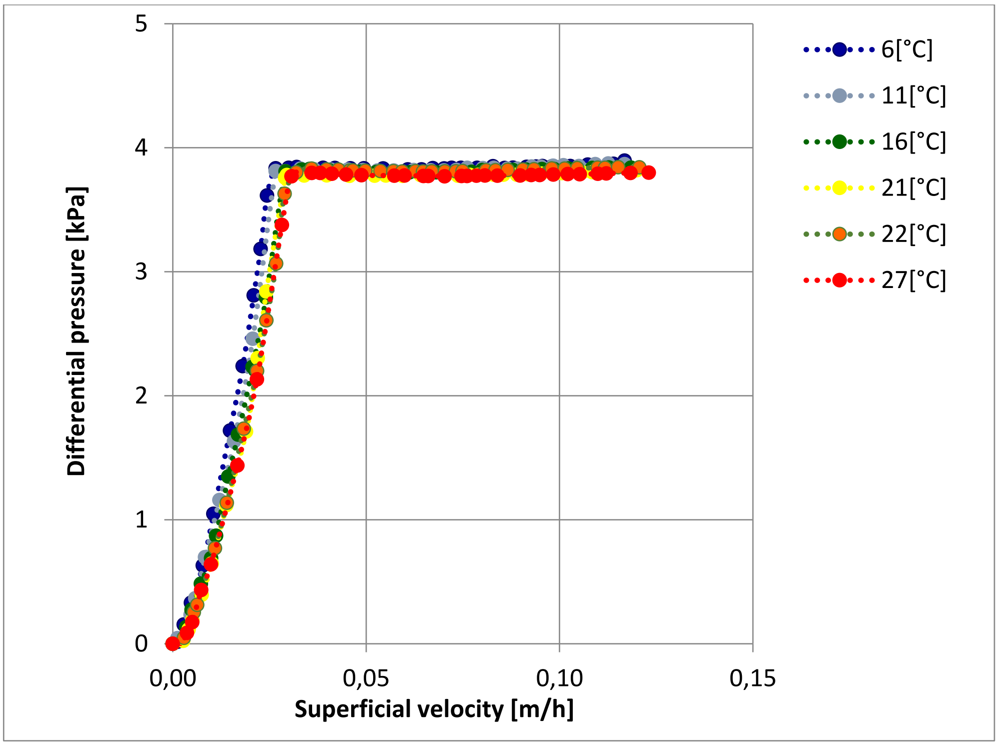

Figure 10: Expansion curve monodispersed spherical glass beads 2.5 mm.

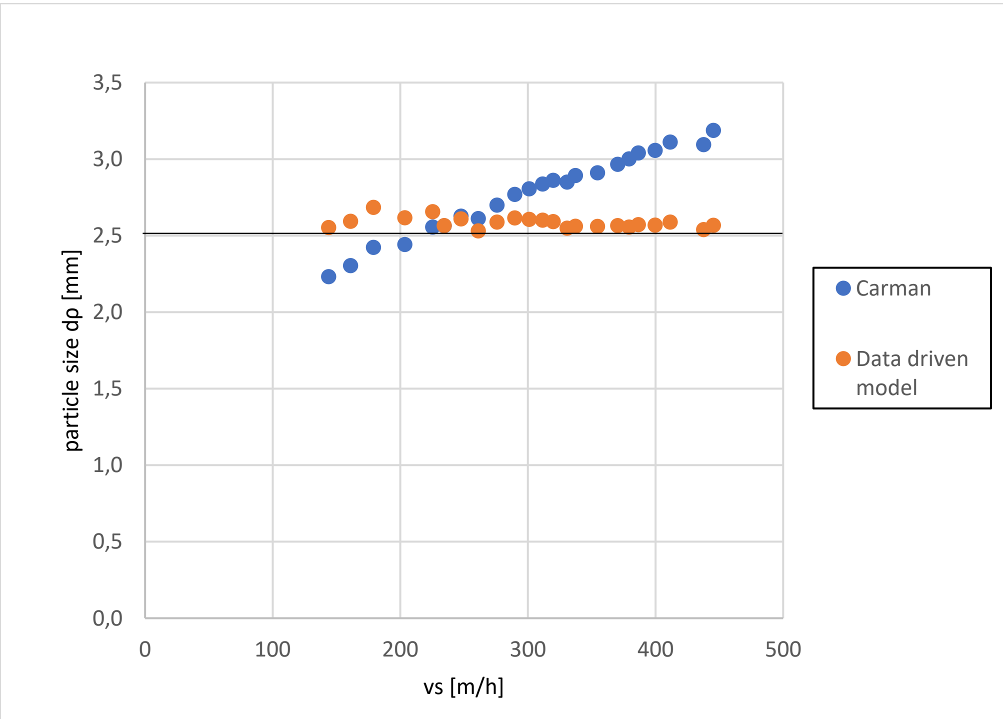

Figure 11: Determination of particle size at an increasing flow rate for monodispersed spherical glass beads 2.5 mm.

Figure 9 illustrates a constant bed height throughout the fixed bed state. However, when fluidisation reaches, a continuous increase in voidage is calculated to a maximum of 0.78 m^3/m^3 at a flow rate of 437 m/h. The measured flow rates are converted to superficial fluid velocity using Equation 4. Whereas, experimentally voidage is calculated using Equation 5. During the experiments, differential pressure is noted from the sensor and it always has shown some deviation in the start but a fixed value is attained afterward, by releasing air, and validation of the sensor gives the difference of almost 2 mbar which is then subtracted from all the noted differential pressure experimental data.

Figure 10, where, v_s [m/h] is plotted against ΔP [kPa] a continuous increase in differential pressure can be observed which supports the literature theory, i.e. if the fluid flow rate upward through a packed bed is increased, the pressure loss in the fluid due to frictional resistance increases after that, a point is reached at which the frictional drag and buoyant force are enough to overcome the downward force exerted on the bed by gravity (O.J.I. Kramer, Boek, & Gridley, 2020), (P.J. de Moel, 2006).

After the graphical exploration of the experimental data and determining the graphical expansion behaviour, prediction models are then calibrated and validated by using experimental data of monodispersed glass beads 2.5 mm at different temperatures. First, voidage is calculated for monodispersed spherical glass beads using the Carman-Kozeny Equation for the fluidised bed (Carman-Kozeny, 1937)

At fluidisation,

$$\frac{\Delta P}{\Delta L} = (\rho_p - \rho_f) g (1 - \varepsilon) \tag{15}$$

Carman-Kozeny Equation:

$$\frac{\Delta P}{\Delta L} = 180 \frac{v_s \eta}{{d_p}^2} \frac{(1-\varepsilon)^2}{\varepsilon^3} + 2.87 \frac{{\rho_f}^{0.9} {v_s}^{1.9} \eta^{0.1}}{{d_p}^{1.1}} \frac{(1-\varepsilon)^{1.1}}{\varepsilon^3} \tag{16}$$

In Equations 15 and 16 left-hand sides are the same so the final Equation will be:

$$(\rho_p - \rho_f) g (1 - \varepsilon) = 180 \frac{v_s \eta}{{d_p}^2} \frac{(1-\varepsilon)^2}{\varepsilon^3} + 2.87 \frac{{\rho_f}^{0.9} {v_s}^{1.9} \eta^{0.1}}{{d_p}^{1.1}} \frac{(1-\varepsilon)^{1.1}}{\varepsilon^3} \tag{17}$$

Secondly, voidage is also calculated using a new empirical data-driven model (O. J. I. Kramer, de Moel, Padding, et al., 2020b)

$$\varepsilon = c_0 {v_s}^{c_1} {v_T}^{c_2} {d_p}^{c_3} \left(\frac{\rho_p}{\rho_f} - 1\right)^{c_4} \tag{18}$$

ε for both Equations 17 and 18, is solved implicitly using Bolzano intermediate value theorem (Apostal, 1967). Substantially, inverting the Carman-Kozeny Equation and data-driven model Equations for the measured voidage, viscosity, and velocity the particle size can be determined too using again Bolzano intermediate value theorem.

4.2 Particle size determination

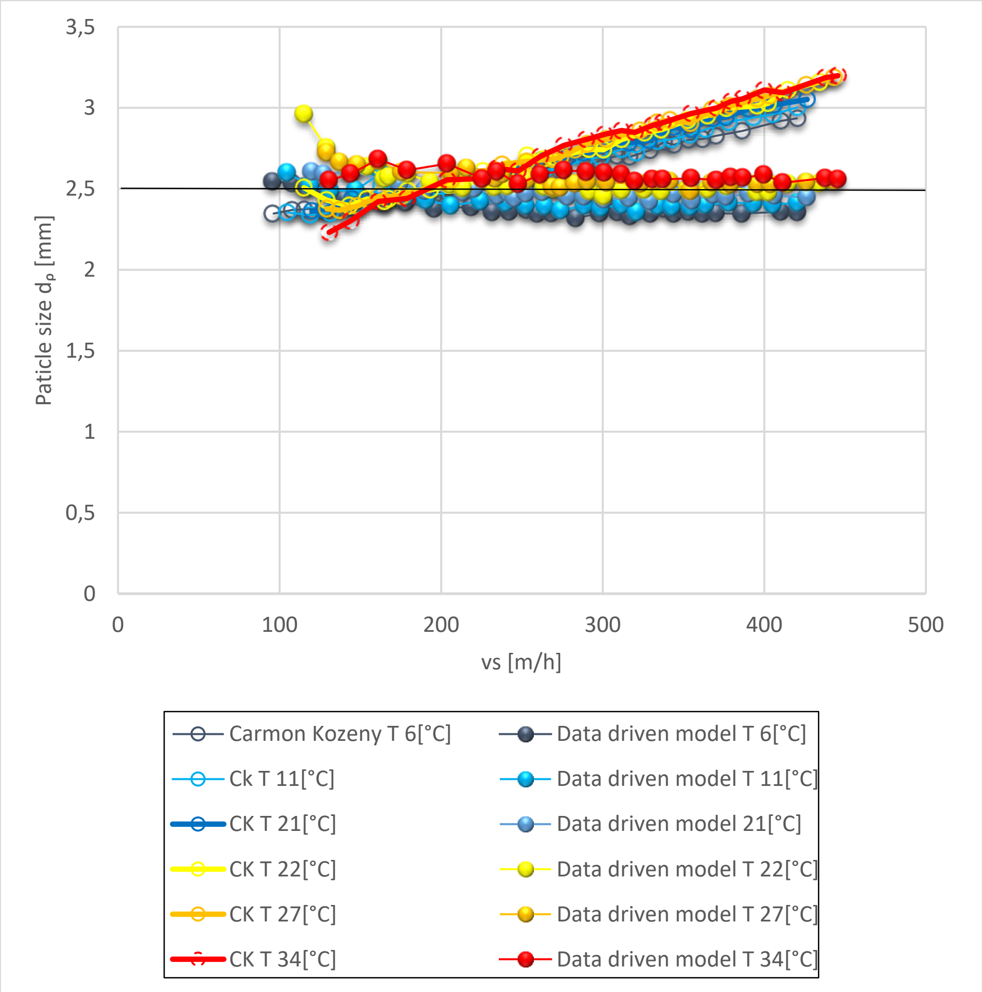

Figure 12: Determination of particle size at an increasing flow rate for monodispersed spherical glass beads at different temperatures.(——) shows actual measured particle diameter 2.5 mm

It is demonstrated from the graphical exploration that for monodispersed glass beads 2.5 mm new empirical data-driven model fits better than the widely used conventional model Carman-Kozeny 1937. Results show that d_p is independent of superficial velocity for a perfectly round shape.

After calculating and validating a new empirical data-driven model for spherical beads, then the expansion behaviour of rods is observed experimentally.

4.3 Graphical exploration glass rods

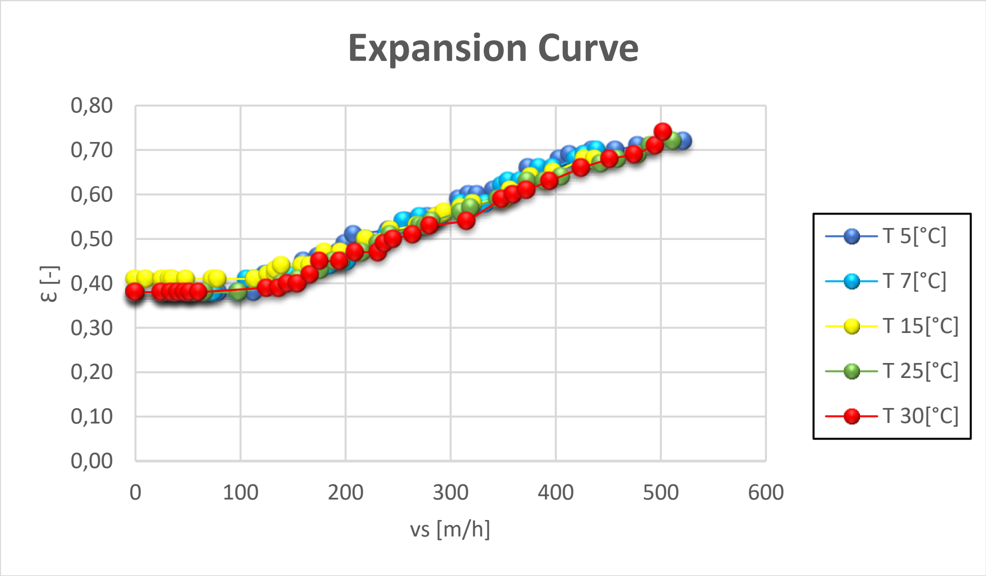

Figure 13: Expansion curve glass rods aspect ratio 3

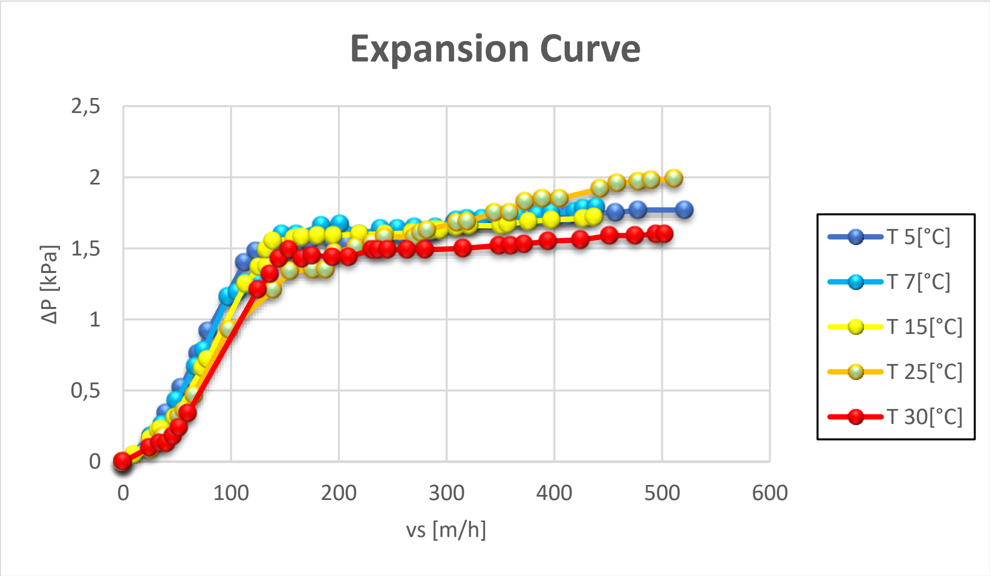

Figure 14: Expansion curve glass rods aspect ratio 3.

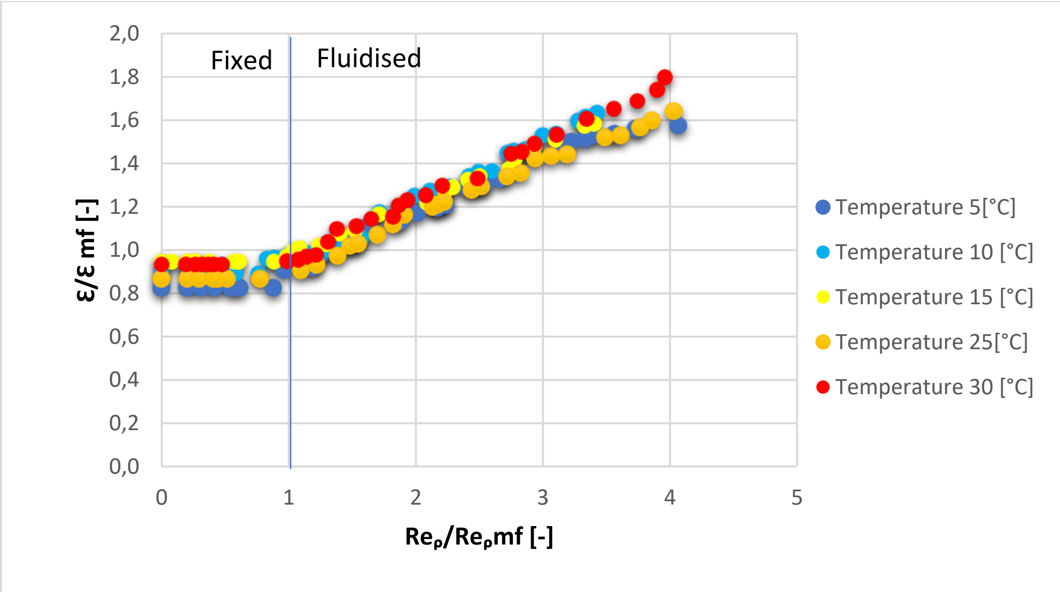

Figure 15: A general dimensionless number approach for glass rod expansion.

The expansion behaviour of rods can be seen in Figure 13, and Figure 14. The overall trend shows a similar expansion behaviour to monodispersed glass beads. A continuous increase in the partial pressure can be observed until the fixed bed state, afterward when fluidisation state reaches the partial pressure difference stays almost constant that supports the theoretical concept of head loss during an expansion (O.J.I. Kramer, Boek, & Gridley, 2020). Slight variations are shown at T ≈ 25 ^{o}C this can be due to unstable flow and deviation of the pressure sensor. As the superficial fluid velocity increases up to ≈ 300 m/h, rod particles tend to fall with the largest projection area normal to the direction of motion. However, rod particles show signs of oscillations and instability in the range of flow 450 – 550 m/h.

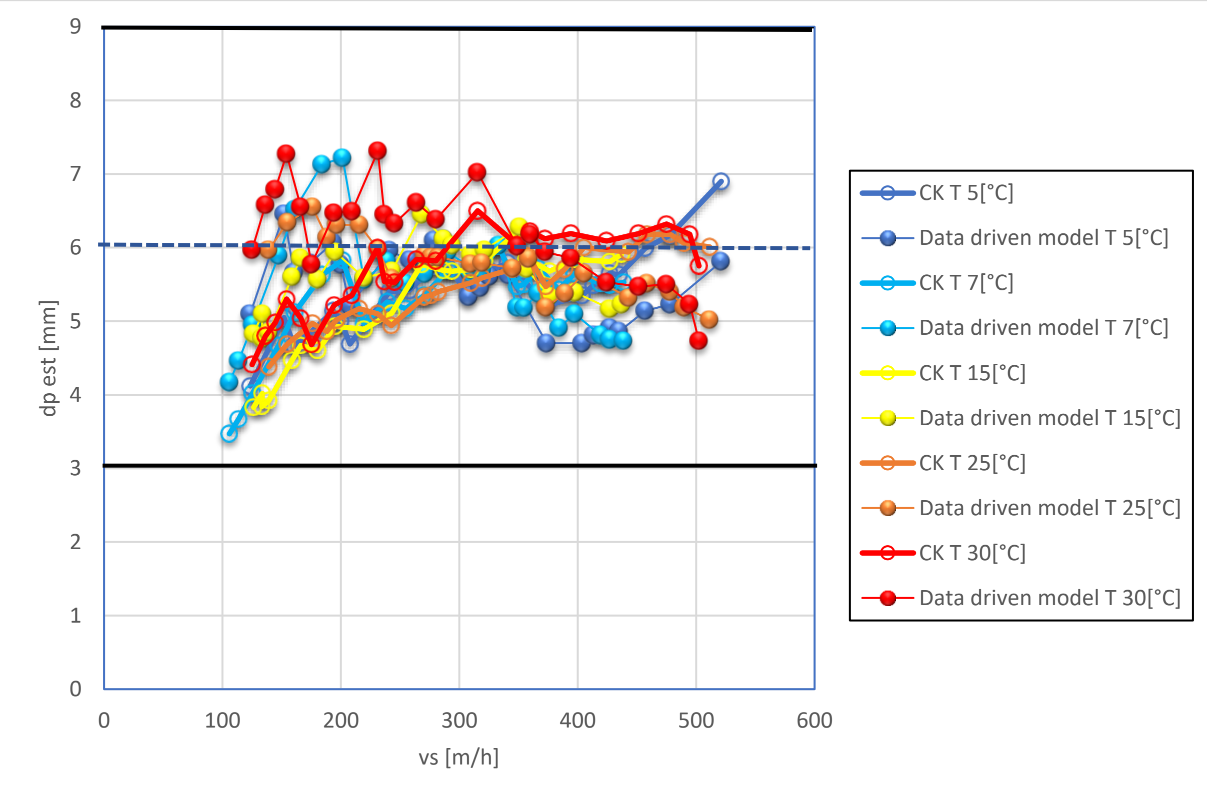

Figure 16: Estimated spherical particle diameter for glass rods. (——) lines refer to boundary conditions 3 mm or 9 mm whereas (--------) indicates an average estimated spherical diameter.

The spherical diameter for glass rods has calculated an average of 6 mm with aspect ratio 3 i.e. (Length/Width), (9 mm/3 mm) by using Carman-Kozeny and empirical data-driven model and can be seen in Figure 16. Theoretically, in a fixed bed state, rods are randomly packed whereas with the increase in velocities they are vertically orientated while at maximum fluidisation they orientate randomly and settled horizontally at the bottom (Magnetic Particle Tracking for Non-spherical Particles in a Cylindrical Fluidised Bed). Figure 17, show experimentally it has observed too that at low flow rates rods are lying randomly but with increasing flow rates they tend to show a preference for an upright orientation referring diameter to be 3 mm afterward with an increase in flow rate they are randomly orientated showing mostly diameter on average to be 6 mm calculated using models and at the settling time, they settled horizontally showing 9 mm diameter but the movement of some particles are affected by the adjacent particles.

Figure 17: Orientation of glass rods with increasing fluid flow rate.

Since, experimental data also shows that, unlike monodispersed spherical beads, d_p for the rod is dependent on the fluid flow rates because it is not constant particle property and it changes with the change in respective superficial fluid velocity. A little variation can be seen due to the wall effects during fluidisation but that can be avoided. Experimental results have also shown that the values for d_p vary from fixed bed state to settling so it is not a constant parameter in the case of non-spherical particles. This factor has also been proven by (O.J.I. Kramer et al., 2021) illustrated (rapid sand filter grains used for backwashing process) that shape factor is not a constant particle property but is also dependent on the fluid properties and it varies along with all the bed states for non-spherical particles. In the case of rods, orientation and particle shape have made it difficult to decide which particle diameter shall be considered as there are two boundary conditions either 3 mm or 9 mm, or the estimated spherical diameter of 6 mm.

So, the first attempt that is a replacement of particle diameter with mathematically defined dimensions in a voidage prediction model is followed using Equation 14. However, this prediction model shows almost 60% relative error to experimental data which specifies inaccuracy of the following model for non-spherical particles (glass rods) whereas, it works well for spherical glass beads. By a pragmatic approach, the model accuracy can be improved by having better and reasonable fit parameters. Subsequently, literature investigation (Agu et al., 2019) has shown that particle diameter, instead of using define dimensions like in present research can be replaced by introducing sphericity (Wadell, 1933) in a voidage prediction model but it is indeed a complex strategy.

4.4 Dimensionless approach

A second approach for non-spherical particles is also considered using the experimental data, that the voidage is also a function of drag. Using dimensionless numbers can cancel out particle diameter which supports the research question. Therefore, this approach is also investigated. In the literature, famous models like Carman-Kozeny, Van Dijk, and Ergun illustrate drag as a function of particle Reynolds number. Since in the case of water the operational field lies in the vicinity of the transitional field, therefore, Carmon-Kozeny drag relation is preferred and laminar/transitional regime (drag at low Reynolds number) will be of interest, and it is found in the academic world, that Kozeny proposed a fixed shape factor K = 180 however it is not constant at higher velocities shown by (Carman-Kozeny, 1937) where he introduced a drag coefficient which can be written in the form of turbulent (f_T) or the laminar form (f_L) as a function of Reynolds number.

Carman-Kozeny theoretical drag (turbulent approach):

$$f_T = \frac{\Delta P}{\Delta L}\frac{d_p}{\rho_f {v_s}^2}\frac{\varepsilon^3}{1-\varepsilon} \quad (19)$$

For Carman-Kozeny theoretical drag (laminar/transitional approach) f_L is calculated by multiplying f_T with Re_ε where Re_ε is a modified particle Reynolds number because in present research laminar regime is of importance rather than turbulent due to it rare applications in liquid-solid fluidisation.

$$f_L = f_T Re_\varepsilon \quad (20)$$

$$Re_\varepsilon = \frac{\rho_f v_s d_p}{\eta}\frac{1}{1-\varepsilon} \quad (21)$$

$$f_L = f_T\, Re_\varepsilon = 180 + 2.87\, {Re_\varepsilon}^{0.9} \quad (22)$$

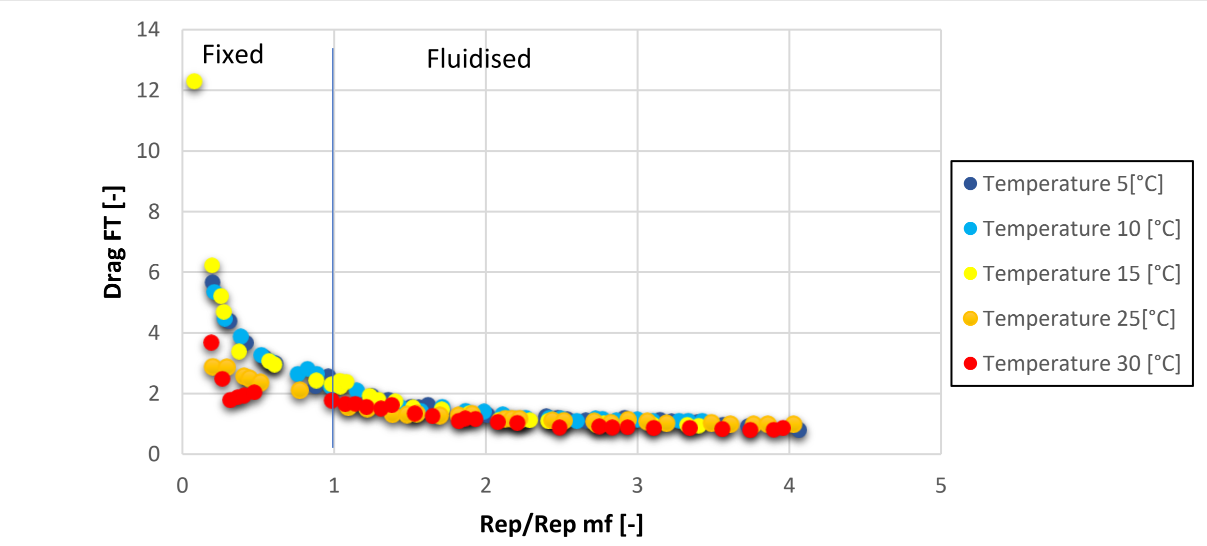

Figure 18: Determination of the dimensionless drag coefficient in the turbulent form.

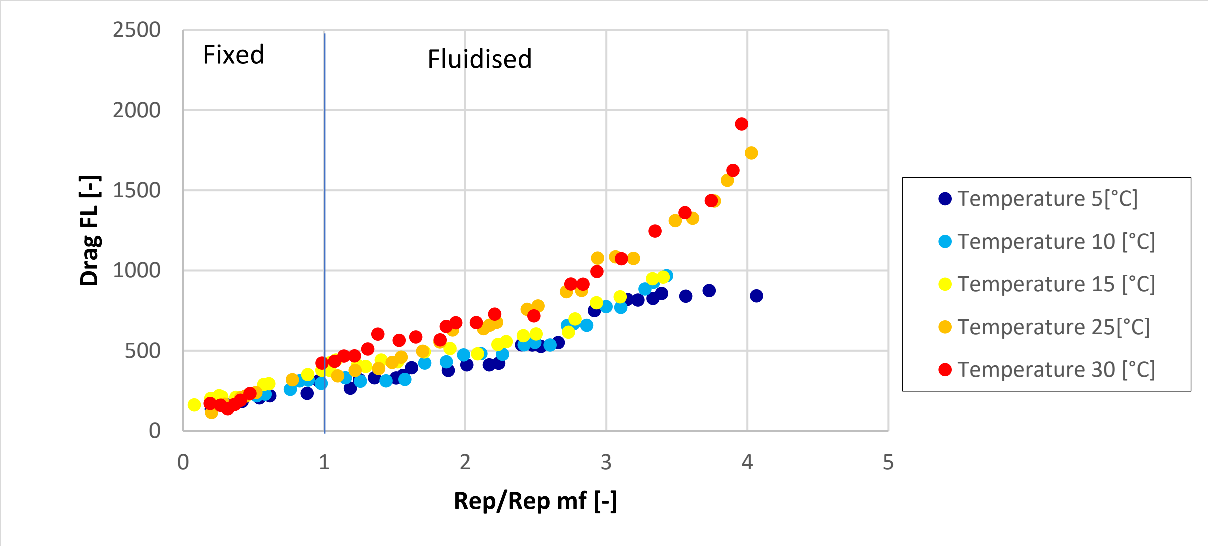

Figure 19: Determination of the dimensionless drag coefficient for laminar form.

Figure 18 and Figure 19, is obtained by plotting drag coefficient f_T ,and f_L in a linear plot, where f_L is the dimensionless coefficient for laminar representation, and f_T is the dimensionless drag coefficient for turbulent representation and Re_p is the modified Reynolds particle number. One of the most common example for drag and Reynolds number is the Moody diagram (Offor & Alabi, 2016). Figure 18, illustrates that the drag decreases with increasing Reynolds number. In most of academic work deviation between experimental and drag model is often hidden by using log-log scale however by taking under consideration Figure 19, where f_L is calculated using Equation 22 shows the clear drag and Reynolds number relation on a linear scale. It also illustrates that Carman drag coefficient at fixed bed state is no more constant, i.e. 180, and is increasing persistently. The drag coefficient reaches almost 450 in the laminar representation which is considerably larger than the well-known Kozeny constant, and the reason behind this is the arrangement of non-spherical particles in a packing position at the fixed bed state.

However to account for voidage in a model the dimensionless approach has shown by (O. J. I. Kramer et al., 2020) where a new dimensionless number namely Froude number has been introduced with Reynolds number as a function of voidage.

4.5 Particle shape factor determination

Another investigation to determine the variability of particle shape factor has been done by using the ratio of the drag coefficient for Carman-Kozeny and the measured drag coefficient f_L. Simultaneously, it is hypothesized that the ratio in Equation 23 is dependent on the hydraulic state that means the ratio of actual modified particle Reynolds number. Whereas, using Bolzano intermediate value theorem, a dynamic shape factor can be determined for various flow rates.

A simplified Equation for determining dynamic shape factor ϕ_s:

$$\phi_s = \sqrt{\frac{f_{L,CK}}{f_L}} \qquad 23$$

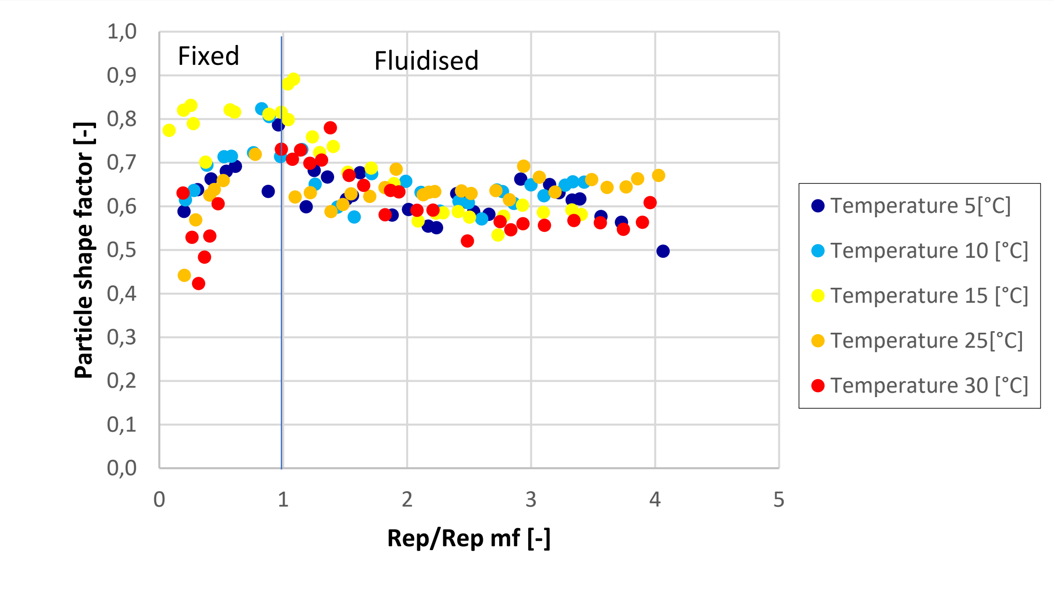

Figure 20: Determination of a dynamic shape factor.

Figure 20, illustrates a dynamic shape factor and explained that the shape factor is also not a constant property for non-spherical particles in both fixed and fluidised bed states. The reason behind exhibiting dynamic shape factor is the random arrangement of particles in a fixed bed state and orientation of the particles during fluidisation state. In the literature and engineering field shape factor approach is applied to compensate non-sphericity only in the fixed bed state however, it is simply emitted in a fluidised state for the same particles

Figure 20, emphasises a dynamic shape factor which is decreasing in fluidisation state and is not constant. It can be seen in the work of (Lau & Chuah, 2013) where the dynamic shape factor for cylinders varies due to retardation of the wall and orientation of the particles. However, in literature, (Magnetic Particle Tracking for Non-spherical Particles in a Cylindrical Fluidised Bed) shape factor for rods of different aspect ratios lies between 0.58 and 0.70 which verifies the determined shape factor for glass rods Figure 20. However at fixed bed state it increases due to irregular arrangements of particles.

Subsequently, it is reinforce by using experimental data of glass rods that the shape factor approach is not suitable for non-spherical particles and it is also not constant in fluidisation state but is a dynamic property. It strengthen graphical and experimental findings too, Figure 16, that the non-spherical particles are dependent on fluid flow rate and particle size is not a constant particle property therefore use of particle diameter in voidage prediction models should be limited.

5 Conclusions

The voidage and particle size are crucial parameters in the drinking water treatment process like pellet-softening and its accurate calculation is of great importance to maintain and provide optimal process conditions in pellet-softening reactors. To determine voidage experimentally for this preliminary hydraulic modelling exploration several expansion experiments were conducted at different temperatures, where monodispersed spherical glass beads and non-spherical glass rods are fluidised. Graphical exploration of particle diameter and expansion results have shown that the monodispersed spherical particles are independent of superficial fluid velocity but are dependent on the temperature. However, in the case of non-spherical particles, a clear dependency on flow has been observed which shows that it is not a constant particle property and varies with increasing flow rate.

Furthermore, particle orientation has also been observed during experimentation and is compared with literature knowledge. It is demonstrated that particles at fixed bed state are randomly packed and they arrange themselves vertically with increasing flow rates but the movement of few particles are affected by their neighbouring particles. Whereas, they orientate and realign at different positions throughout the fluidisation. Therefore, it is difficult to account for non-spherical particles in terms of their particle size and shape in a voidage prediction model in a fairly fluidised state. This is something always elucidated in the literature too. Non-spherical particles have different aspects to consider during fluidisation that includes particle shape, orientation, and surface roughness compared to the spherical particles.

In this particular research, several approaches have been followed to investigate how to account for particle size for non-spherical particles. A preliminary approach in a voidage prediction model has shown for the replacement of particle diameter with the defined dimensions (width and length). another attempt to account for voidage using dimensionless numbers has also been investigating. Furthermore in operational fields fixed pore shape factor are applied to compensate non-sphericity of the granules and is widely used in a voidage prediction models. Therefore, another attempt to account for voidage using dimensionless numbers has also been investigated This approach is helpful to conclude that the Carman-Kozeny constant cannot be considered constant for non-spherical particles (rod shaped glass) in the fixed bed state due to the rearrangement of non-spherical particles in a packing position. Non-spherical particles experience anisotropic drag in a fixed and fluidised state because of the surrounding fluid and interactions with the adjacent particles. Additionally, it is also explained that various shape factors for the same particles are illustrated not even in fixed bed state but also at fluidisation state. Therefore, the use of constant shape factors regarding irregular and natural particles is not recommended because natural particles are also not completely spherical in shape.

6 Recommendations

In a water treatment full-scale installation with continuous challenge, plant-wide control, and complex models for optimal numerical solutions are less desirable. That is why explicit effective models able to predict voidage accurately under all multiphase phenomena and many other non-ideal conditions are favoured. Therefore, for future research, it is recommended to take into account a more deep understanding of the orientation angle with which non-spherical particles orientate from one position to the other. This is possible with the use of sophisticated instruments like a 3D scanner, imagej, or any particle tracking technique. However, it is also recommended for future research to use sphericity introduced by (Wadell, 1933) to account for particle shape and size in the voidage prediction model instead of using defined dimensions of the non-spherical particle. For the orientation part inspiring work by (Hölzer & Sommerfeld, 2008) should take into account. So, instead of using a 2D approach, a 3-dimensional approach can be useful. If rods will be the only option then, it is recommended to use rods of smaller sizes in the future experimental work with aspect ratios 1 and 2, and then the results can be compared with experimental data of aspect ratio 3.

In practise and operational fields, granules are often considered more spheres but present research has shown that the non-spherical granules cannot be considered as spheres by applying a constant shape factor. Therefore, there is a need for a more general approach for the future in case if new particles of different shapes will be used in the process so, using particle diameter is not recommended, and their should be any replacement for particle diameter.

During the experimental work, the pressure sensor was not so accurate so it also recommended for future work to take this factor into account and start the experiment by using a bigger pump to release air as most as possible. This helps to bring partial pressure difference to a minimum of 2 mbar, which can be subtracted afterward from the noted pressure difference values. Maintaining the temperature of the water is also of extreme importance to conduct experiments at a required specific temperature so a mobile thermometer is recommended to be used constantly. If the temperature is high enough then the circulation pump can be stopped and cold water can be added manually to maintain the temperature inside of the tank.

7 References

Agu, C. E., Pfeifer, C., & Moldestad, B. M. E. (2019). Prediction of void fraction and minimum fluidization velocity of a binary mixture of particles: Bed material and fuel particles. *Powder Technology*, *349*, 99–107. https://doi.org/10.1016/j.powtec.2019.03.027

Akgiray, O., & Soyer, E. (2006). An evaluation of expansion equations for fluidized solid–liquid systems. *Journal of Water Supply: Research and Technology-Aqua*, *55*(7–8), 517–526. https://doi.org/10.2166/aqua.2006.040

Albright, L. (2008). *Albright's Chemical Engineering Handbook*.

Apostal, T. M. (1967). *Calculus* (2nd ed., Vol. 1).

Bagheri, G., & Bonadonna, C. (2016). On the drag of freely falling non-spherical particles. *Powder Technology*, *301*, 526–544. https://doi.org/10.1016/j.powtec.2016.06.015

Beeftink, M., Hofs, B., Kramer, O., Odegard, I., & van der Wal, A. (2021). Carbon footprint of drinking water softening as determined by life cycle assessment. *Journal of Cleaner Production*, *278*, 123925. https://doi.org/10.1016/j.jclepro.2020.123925

Carman-Kozeny, P. C. (1937). *Fluid flow through granular beds* (pp. 32–48). https://doi.org/10.1016/S0263-8762(97)80003-2

Civan, F. (2007). Critical Modification to the Vogel−Tammann−Fulcher Equation for Temperature Effect on the Density of Water. *Industrial & Engineering Chemistry Research*, *46*(17), 5810–5814. https://doi.org/10.1021/ie070714j

Dharmarajah, A. H. (1982). *Effect of particle shape on prediction of velocity-voidage relationship in fluidized solid-liquid systems* (p. 6314514) [Doctor of Philosophy, Iowa State University, Digital Repository]. https://doi.org/10.31274/rtd-180813-5307

Di Felice, R. (1995). Hydrodynamics of liquid fluidisation. *Chemical Engineering Science*, *50*(8), 1213–1245. https://doi.org/10.1016/0009-2509(95)98838-6

Epstein, N. (2002). Applications of Liquid-Solid Fluidization. *International Journal of Chemical Reactor Engineering*, *1*(1). https://doi.org/10.2202/1542-6580.1010

Ergun, S. (1952). Fluid flow through packed columns. In *Chem.Eng.Sci* (pp. 89–94). https://doi.org/citeulike-article-id:7797897.

Gibilaro, L. G. (2001). *Fluidization Dynamics*. Elsevier.

Graveland, A., Dijk, J., de Moel, P., & Oomen, J. (1983a). Developments in water softening by means of pellet reactors. *Journal American Water Works Association - J AMER WATER WORK ASSN*, *75*, 619–625. https://doi.org/10.1002/j.1551-8833.1983.tb05247.x

Graveland, A., Dijk, J., de Moel, P., & Oomen, J. (1983b). Developments in water softening by means of pellet reactors. *Journal American Water Works Association - J AMER WATER WORK ASSN*, *75*, 619–625. https://doi.org/10.1002/j.1551-8833.1983.tb05247.x

Hölzer, A., & Sommerfeld, M. (2008). New simple correlation formula for the drag coefficient of non-spherical particles. *Powder Technology - POWDER TECHNOL*, *184*, 361–365. https://doi.org/10.1016/j.powtec.2007.08.021

Introduction to Fluidization. (n.d.). 23.

Kramer, O., boek, E., & Gridley, B. (2020). *Expansion Column Vitual Lab*. file:///C:/Users/Eigenaar/Downloads/PBL7-FBR-%20Virtual%20lab%20-%20Expansion%20column%20manual-OK-EB-QMUL-v1.41%20(1).pdf

Kramer, O., de Moel, P., Padding, J., Baars, E., El Hasadi, Y., & Boek, E. (2020). Accurate voidage prediction in fluidisation systems for full-scale drinking water pellet softening reactors using data driven models. *Journal of Water Process Engineering*, *37*, 101481. https://doi.org/10.1016/j.jwpe.2020.101481

Kramer, O., de Moel, P., Raaghav, S., Baars, E., Vugt, W. H., Breugem, W.-P., Padding, J., & Hoek, J. (2020). *Can terminal settling velocity and drag of natural particles in water ever be predicted accurately?* https://doi.org/10.5194/dwes-2020-30

Kramer, O. J. I., de Moel, P. J., Padding, J. T., Baars, E. T., Hasadi, Y. M. F. E., Boek, E. S., & van der Hoek, J. P. (2020a). Accurate voidage prediction in fluidisation systems for full-scale drinking water pellet softening reactors using data driven models. *Journal of Water Process Engineering*, *37*, 101481. https://doi.org/10.1016/j.jwpe.2020.101481

Kramer, O. J. I., de Moel, P. J., Padding, J. T., Baars, E. T., Hasadi, Y. M. F. E., Boek, E. S., & van der Hoek, J. P. (2020b). Accurate voidage prediction in fluidisation systems for full-scale drinking water pellet softening reactors using data driven models. *Journal of Water Process Engineering*, *37*, 101481. https://doi.org/10.1016/j.jwpe.2020.101481

Kramer, O. J. I., Padding, J. T., van Vugt, W. H., de Moel, P. J., Baars, E. T., Boek, E. S., & van der Hoek, J. P. (2020). Improvement of voidage prediction in liquid-solid fluidized beds by inclusion of the Froude number in effective drag relations. *International Journal of Multiphase Flow*, *127*. https://doi.org/10.1016/j.ijmultiphaseflow.2020.103261

Kramer, O. J. I., van Schaik, C., Hangelbroek, J. J., de Moel, P. J., Colin, M. G., Amsing, M., Boek, E. S., Breugem, W. P., Padding, J. T., & van der Hoek, J. P. (2021). A novel sensor measuring local voidage profile inside a fluidised bed reactor. *Journal of Water Process Engineering*, 102091. https://doi.org/10.1016/j.jwpe.2021.102091

Kramer, Onno J. I., de Moel, P. J., Padding, J. T., Baars, E. T., Rutten, S. B., Elarbab, A. H. E., Hooft, J. F. M., Boek, E. S., & van der Hoek, J. P. (2021). New hydraulic insights into rapid sand filter bed backwashing using the Carman–Kozeny model. *Water Research*, *197*, 117085. https://doi.org/10.1016/j.watres.2021.117085

Lau, R., & Chuah, H. (2013). Dynamic shape factor for particles of various shapes in the intermediate settling regime. *Advanced Powder Technology*, *24*, 306–310. https://doi.org/10.1016/j.apt.2012.08.001

Maeng, S. K., Salinas Rodriguez, C. N., Choi, J., Kim, S.-H., Yu, Y., Kim, B.-S., & Hong, S. W. (2016). Organic micropollutant removal from groundwater: Comparison of pellet softening and nanofiltration. *Journal of Water Supply: Research and Technology—AQUA*, *65*(6), 453–464.

Magnetic particle tracking for nonspherical particles in a cylindrical fluidized bed. (n.d.). Retrieved 8 June 2021, from https://www.ncbi.nlm.nih.gov/pmc/articles/PMC5703443/

Moghaddam, E. M., Foumeny, E. A., Stankiewicz, A. I., & Padding, J. T. (2019). Fixed bed reactors of non-spherical pellets: Importance of heterogeneities and inadequacy of azimuthal averaging. *Chemical Engineering Science: X*, *1*, 100006. https://doi.org/10.1016/j.cesx.2019.100006

Offor, U. H., & Alabi, S. B. (2016). An Accurate and Computationally Efficient Explicit Friction Factor Model. *Advances in Chemical Engineering and Science*, *6*(3), 237–245. https://doi.org/10.4236/aces.2016.63024

P.J.de Moel. (2006). *Drinking water Principles and Practices*.

Richardson-Zaki, J. F., W. N. (1954). *Sedimentaion and Fluidization* (pp. 35–53). https://doi.org/10.1016/S0263-8762(97)80006-8

Rietveld, L. C., Schagen, K., & Kramer, O. (2006a, January 29). *Optimal operation of the pellet softening process*. American Water Works Association Inorganic Contaminants.

Rietveld, L. C., Schagen, K. van, & Kramer, O. J. I. (2006b). Optimal Operation of the Pellet Softening Process. *AWWA Inorganic contaminants workshop*, 1–14. https://research.tudelft.nl/en/publications/optimal-operation-of-the-pellet-softening-process

River basin management—Water—Environment—European Commission. (n.d.). Retrieved 17 February 2021, from https://ec.europa.eu/environment/water/water-framework/index_en.html

Schetters, M. J. A., Kramer, O., Kors, L. J., Palmen, L. J., Hofs, B., & Koppers, H. (2015). Circular economy in drinking water treatment: Reuse of ground pellets as seeding material in the pellet softening process. *Water Science & Technology*, *71*, 479–486. https://doi.org/10.2166/wst.2014.494

Sobhan, R. (2019). *An improved kinetic model and optimized configurations for pellet softening: Modeling and optimization of pellet softening process in drinking water treatment*. https://repository.tudelft.nl/islandora/object/uuid%3A03bd9e7a-22a4-4755-8ee0-35d99e5f2b4f

Soyer, E., & Akgiray, Ö. (2009). A New Simple Equation for the Prediction of Filter Expansion during Backwashing. *Journal of Water Supply Research and Technology-Aqua - J WATER SUPPLY RES TECHNOL-AQ*, *58*. https://doi.org/10.2166/aqua.2009.090

van der Hoek, J. P. (2012). Towards a climate neutral water cycle. *Journal of Water and Climate Change*, *3*(3), 163–170. https://doi.org/10.2166/wcc.2012.015

Van Schagen, K. M. (2009). *Model-Based Control of Drinking-Water Treatment Plants*. https://repository.tudelft.nl/islandora/object/uuid%3Afc4d865d-1ed7-409e-83ba-6270dacdec67

van Schagen, K., Rietveld, L., Babuška, R., & Baars, E. (2008). Control of the fluidised bed in the pellet softening process. *Chemical Engineering Science*, *63*(5), 1390–1400. https://doi.org/10.1016/j.ces.2007.07.027

Wadell, H. (1933). Sphericity and Roundness of Rock Particles. *The Journal of Geology*, *41*(3), 310–331. https://doi.org/10.1086/624040

Wen, C. Y., & Yu, Y. H. (1966). A generalized method for predicting the minimum fluidization velocity. *AIChE Journal*, *12*(3), 610–612. https://doi.org/10.1002/aic.690120343

Who we are-Waternet. (n.d.). Retrieved 17 February 2021, from https://www.waternet.nl/en/about-us/who-we-are/

Yang, W.-C. (2003a). *Handbook of Fluidization and Fluid-Particle Systems*. CRC Press.

Yang, W.-C. (2003b). Handbook of Fluidization and Fluid–Particle System. *China Particuology*, *1*, 137–137. https://doi.org/10.1016/S1672-2515(07)60126-2

Yang, W.-C. (2003c). Handbook of fluidization and fluid-particle systems. *China Particuology*, *1*(3), 137. https://doi.org/10.1016/S1672-2515(07)60126-2

8 Supplementary Material

8.1 Experimental setup

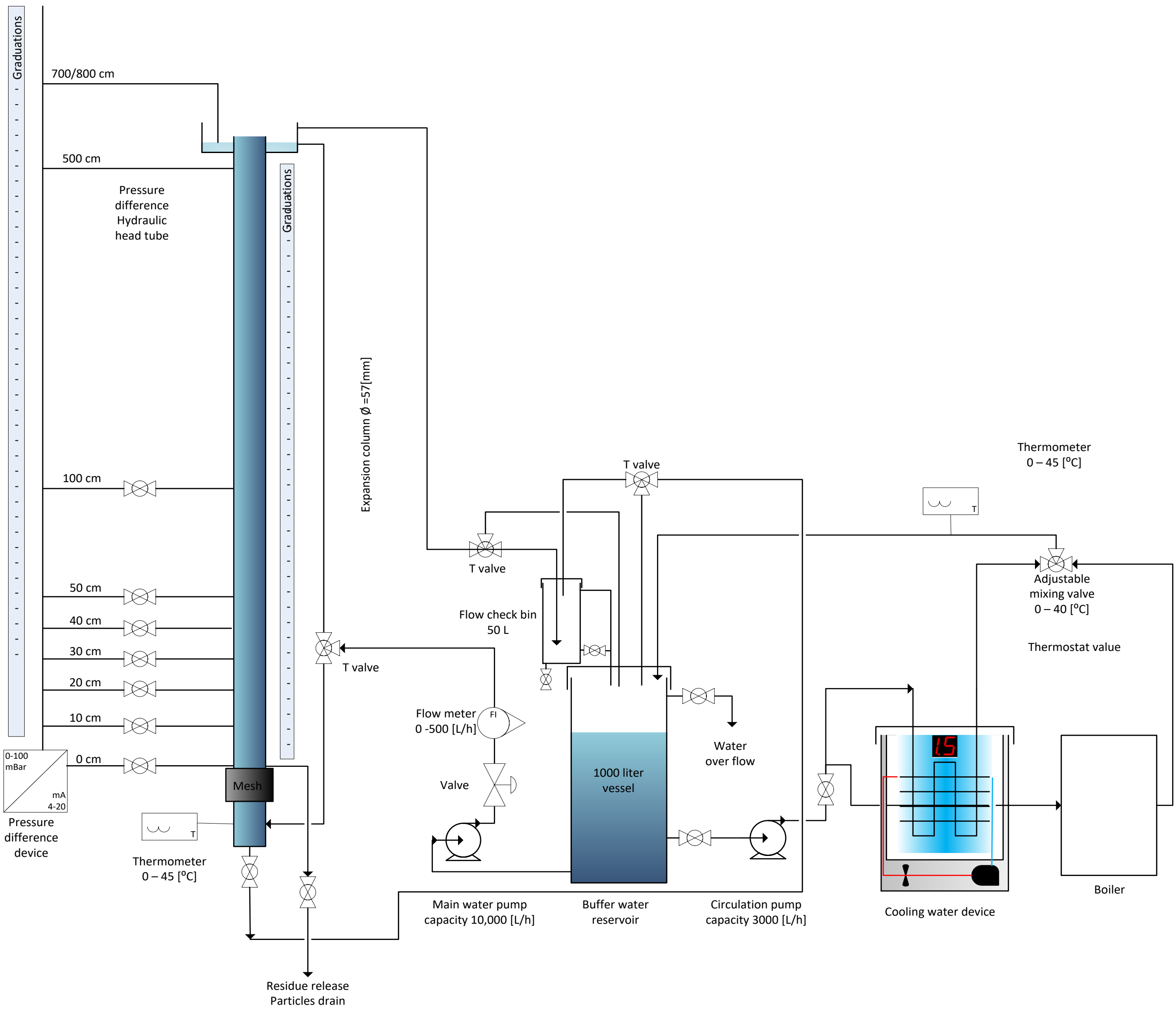

Figure 21: P&ID Expansion column (O.J. I. Kramer, de Moel, Padding, et al., 2020b).

8.2 Practical Density

To measure particle density pycnometer is used. In the beginning, the pycnometer is always calibrated and after that, it is partially filled with beads and is weighed after that it is filled with water and beads and is weighed again. The density of water at room temperature is a known factor so using the information of water mass and density the volume of water is determined which is then helpful to determine the volume of beads using this all known information density of beads is calculated. The method is revised 10 times and the excel template is used to save all the data.

		m_c	m_{cw}	m_{cp}	m_{cpw}	m_p	m_w	V_w	V_p	ρ_p
Sample type	Nr. [#]	maass measuring cyl empty [g]	Mass measuring cylir water [g]	weighed mass measuring cylinder + beads [g]	weighed mass measuring cylinder +beads+water [g]	Mass weighed beads [g]	Mass water [g]	Volume measurii water [mL]	Volume after rem water+ n [mL]	similarly mass beads [kg/m³]
Glass beads PWN	1	31	83	103	127	72	23	23	29	2,479
	2	31	83	105	128	74	23	23	30	2,476
	3	31	83	107	128	76	21	21	31	2,439
	4	31	83	105	128	74	22	22	30	2,475
	5	31	83	107	129	76	22	22	31	2,470
	6	31	83	106	128	75	22	22	30	2,477
	7	31	83	108	129	76	22	22	31	2,475
	8	31	83	107	129	76	22	22	31	2,481
	9	31	83	105	128	74	22	22	30	2,475
	10	31	83	106	128	75	22	22	31	2,463
		31	83						Max =	2,481
		31	83						Min =	2,439
		31	83						mean value =	2,471
									Stdev =	12
				ρ_w =	1,000	[kg/m³]			% =	0.5%
				η =	0.0013	[Pas]				
				V_c =	52	[mL]				
				T =	11	[ºC]				

Figure : -Particle density measurements of glass beads using a pycnometer

Sample type	Nr. [#]	Mass cylinder empty [g]	Mass cylinder+ water [g]	Weighed Mass cylinder+ +beads [g]	Weighed Mass cylinder+ +beads+water [g]	Weighed Mass Beads [g]	Mass water [g]	Volume cylinder water [mL]	Volume verplaatst water [mL]	mass Beads [kg/m³]
Glass rods	1	32	81	72	104	40	32	32	18	2,213
	2	32	81	90	113	58	23	23	26	2,197
	3	32	81	76	106	44	30	30	20	2,194
	4	32	81	88	112	56	24	24	26	2,192
	5	32	81	81	108	49	28	28	22	2,201
	6	32	81	86	111	55	25	25	25	2,152
	7	32	81	78	107	47	28	28	21	2,171
	8	32	81	88	112	57	24	24	26	2,177
	9	32	81	89	112	57	23	23	26	2,163
	10	32	81	90	113	58	23	23	27	2,184

Resultaten		
Max =	2,213	[kg/m³]
Min =	2,152	[kg/m³]
Gemiddelde =	2,184	[kg/m³]
Stdev =	19	[kg/m³]
% =	0.9%	[-]

Kalibratie pycnometer		
Mass empty picnometer	31.55	[g]
Mass pycnometer with water	81.40	[g]
Mass water pycnometer	49.85	[g]
Density of water	0.9993	[g/cm³]
Volume pycnometer	49.88	[cm³]

ρ_w =	999	[kg/m³]
η =	0.0012	[Pas]
V_c =	50	[mL]
T =	14	[ºC]

$$\rho_w = \frac{999{,}83952 + 16{,}945176 * T - 7{,}9870401 * 10^{-3} * T^2 - 46{,}170461 * 10^{-6} * T^3 + 105{,}56302 * 10^{-9} * T^4 - 280{,}54253 * 10^{-12} * T^5}{1 + 16{,}87985 * 10^{-3} * T}$$

Figure 22: Density measurements of glass rods using a pycnometer

8.3 Particle diameter analysis

Particle diameter is measured for glass rod by using micrometre. Sieve analysis is not done due to its inaccurate result. Rods can pass through the lower sieves and overall it can give a particle diameter but particle shape is distorted. Therefore using micrometer width and length of each rod is measured and 40 values are taken to measured the mean values.

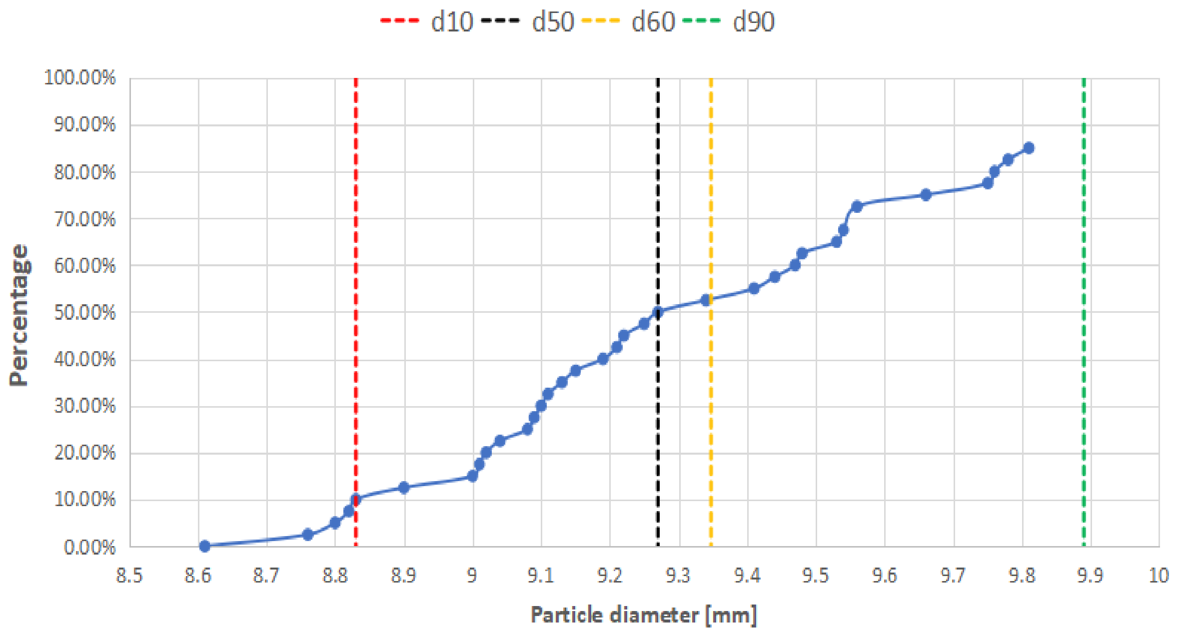

Figure 23: Particle diameter analysis for glass rod length using micrometre.

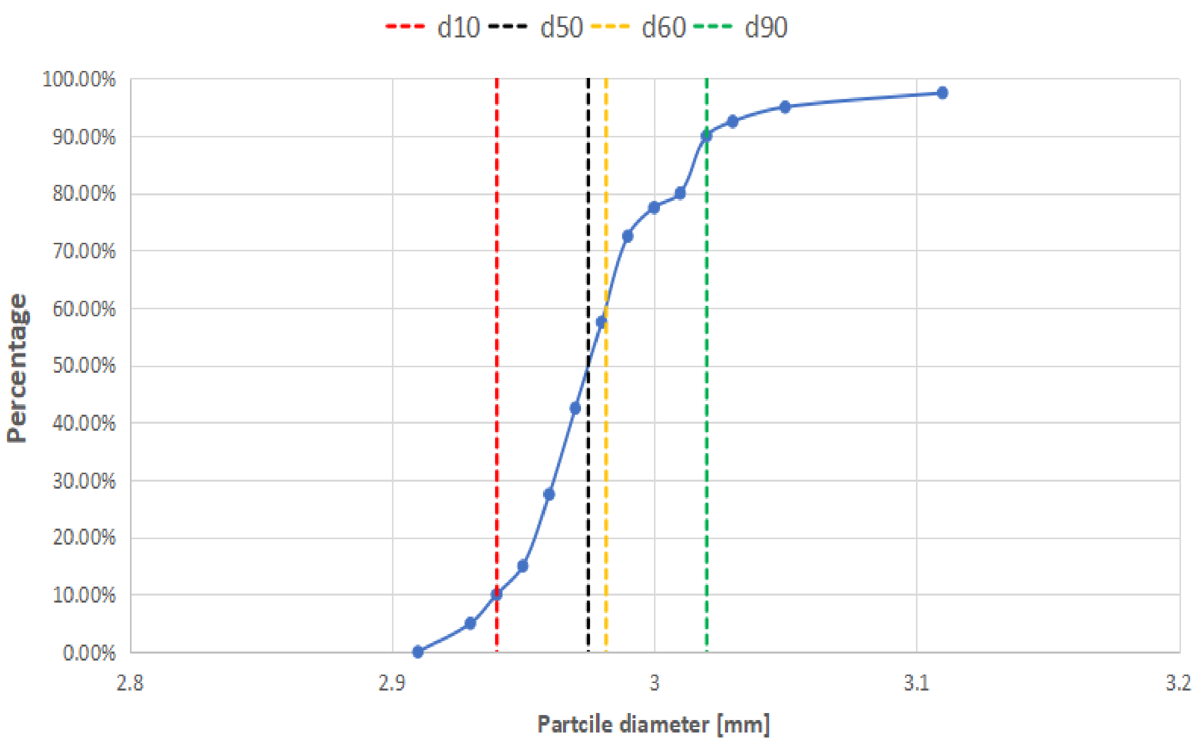

Figure 24: Particle diameter analysis for glass rod width using micrometer.

8.4 Excel Template

An excel template is used to save all the noted experimental data such as water flow rate, temperature, differential pressure and bed height which is then used to calculate voidage and superficial fluid velocity and all the experimental data is useful to calibrate and validate required models.

	Status bed [0/1/2/3]	Water flow Qw [L/h]	Bed height L [m]	Temperature T [°C]	Pressure differ ΔP(399cm) [mbar]	ΔP(399cm) [cm H2O]	Notes of experiments Please make many note about what you see. In case of observed deiavtion pplease use ±.
1	0	0.0	0.22	15.7	2.01		Foto 1 --> luchtbellen op bollen , fixed bed state
2	0	26.2	0.22	15.7	2.53		
3	0	64.4	0.22	15.7	3.60		
4	0	83.6	0.22	15.7	4.25		
5	0	90.0	0.22	15.7	4.35		
6	0	122.6	0.22	15.7	5.14		
7	0	187.4	0.22	15.6	8.65		
8	0	199.3	0.22	15.5	9.23		
9	0	289.6	0.22	15.5	14.53		
10	1	322.3	0.22	15.5	15.68		
11	1	341.0	0.22	15.5	15.69		
12	1	340.0	0.22	15.4	16.87		rods at surface start to jump and align
13	1	355.0	0.23	15.4	17.52		
14	1	405.0	0.23	15.4	17.72		Video 1 (Video 1_19102018.MOV)
15	1	424.0	0.23	15.4	17.84		
16	1	460.0	0.24	15.5	17.89		
17	1	498.2	0.24	15.5	17.92		rods at one side on the surface starts fluidizing
18	1	560.0	0.26	15.7	17.99		
19	1	620.0	0.27	15.7	18.02		
20	1	684.0	0.27	15.7	18.10		Video 2 (Video 2_19102018.MOV)
21	1	731.0	0.28	15.7	18.34		
22	1	750.2	0.29	15.7	18.34		
23	1	790.0	0.30	15.5	18.52		
24	1	820.0	0.30	15.5	18.57		
25	1	895.0	0.31	15.6	18.64		
26	1	910.0	0.33	15.6	18.75		
27	1	960.0	0.35	15.6	18.92		
28	1	1,015.1	0.36	15.6	19.02		
29	1	1,090.0	0.39	15.5	19.10		
30	1	1,115.0	0.40	15.5	19.16		
31	n.a.						
32	n.a.						
33	n.a.						
34	n.a.						
35	n.a.						
36	n.a.						
37	n.a.						
38	n.a.						
39	n.a.						
40	n.a.						

Figure 25: Excel template to feed in experimental data.

8.5 Expansion Curves

These are expansion curves compose from experimental data for monodispersed glass beads 3.5 mm.

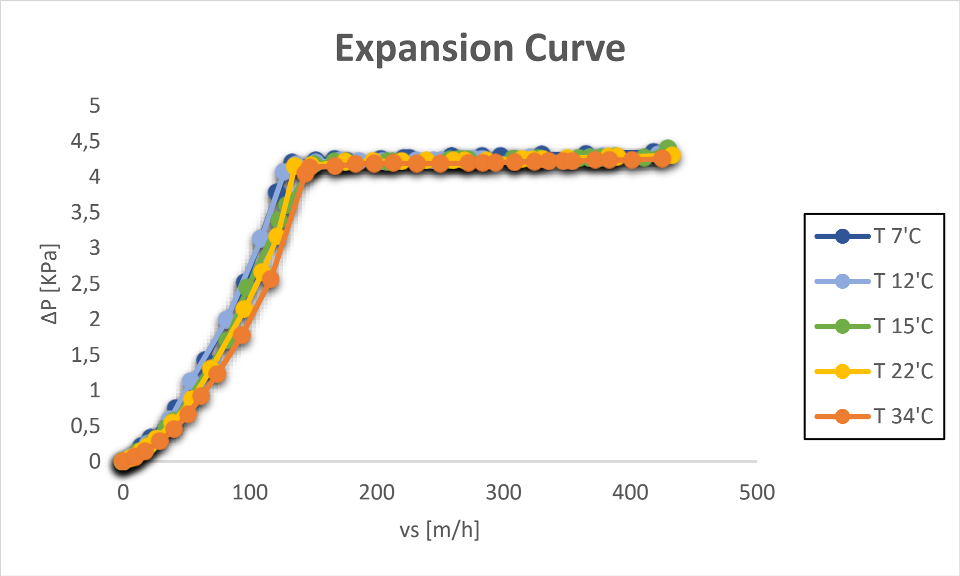

Figure 26: Expansion curve glass beads 3.5 [mm].

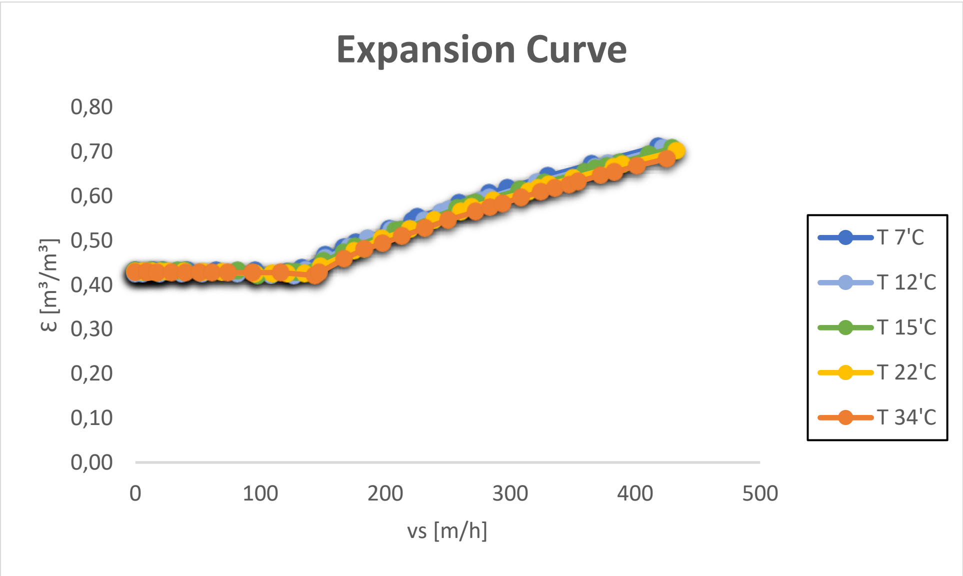

Figure 27: Expansion curve glass beads 3.5 [mm].

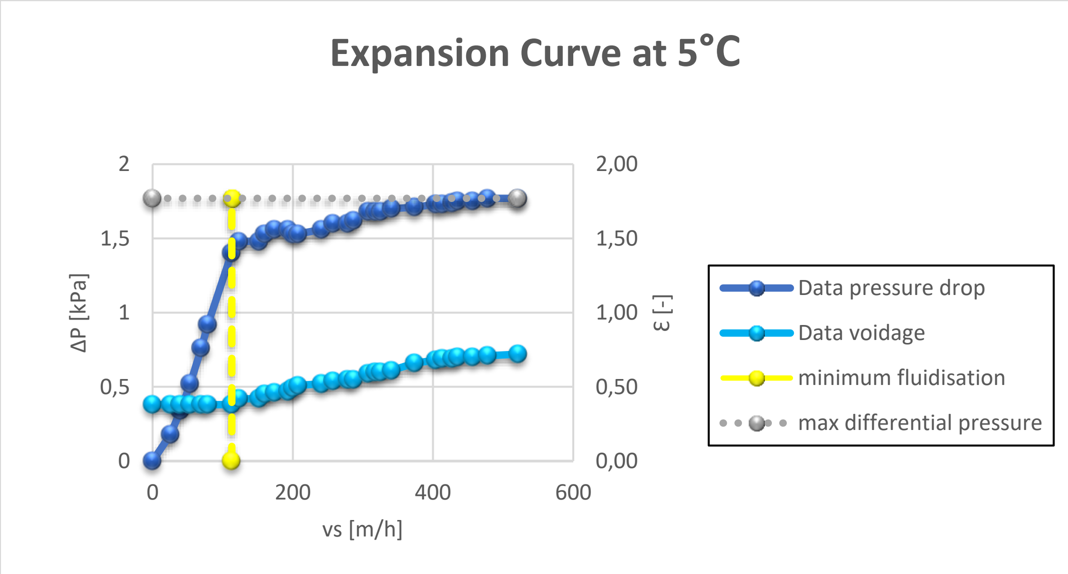

Figure 28: Expansion curve glass rods.

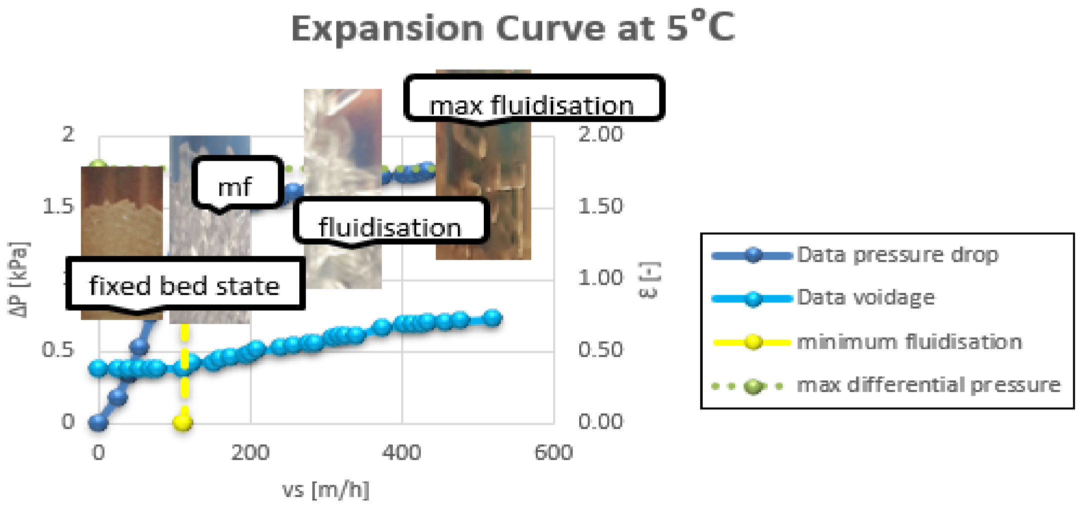

Figure 29: Expansion curve glass rods with orientation.

It has been observed during experiments that at minimum fluidisation particles orientate vertically having a projected diameter of 3mm, whereas, at fluidisation state, they have a spherical diameter of approximately 6mm. However, rod particles settle horizontally having a diameter of 9mm.

To calculate the angle of orientation by which a particle orientate in fluidize state following assumptions have been done.

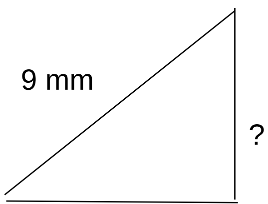

6mm

Figure 30 orientation of rod particle in a fluidised state

Hypothesis = 6mm

Adjacent = 9mm

The opposite can be calculated then:

$(6)^2+x^2 = (9)^2$

X = 6.7mm

Tan α = opposite/ Adjacent

therefore,

$\alpha = \tan^{-1}$ Opposite/Adjacent

$\alpha = \tan^{-1}$ 7.6 mm/ 6mm

α= 1.26

8.6 Dynamic shape factor

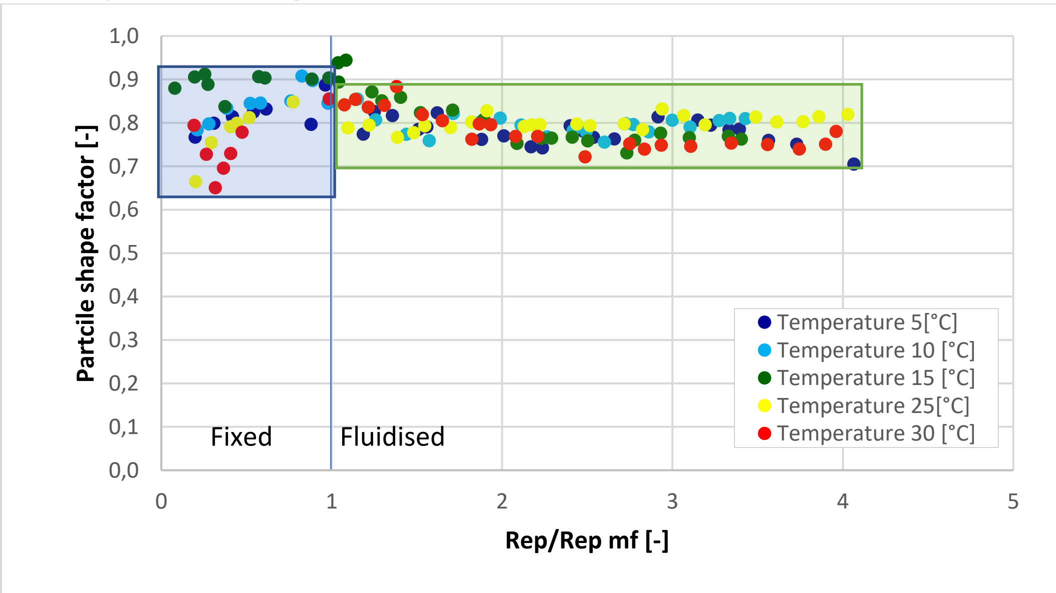

Figure 31: Dynamic shape factor determination